Tetrazine-Enhanced Donor-Acceptor-Donor Photosensitive Metal-Organic Frameworks for Combating Drug-Resistant Bacteria and Accelerating Diabetic Wound Healing

Yanzhao Chen[a,b], Yangyin Xue[b], Xiaowei Xu[b], Yu Su[a], Long Zhu[b], Yifei Zuo[b], Chao Ban[b], Wancai Que[c*], Yueqin Zheng [b*], Weiwei Guo[a*]
[a] School of Science, China Pharmaceutical University, Nanjing 211198, China
[b] Center of Drug Discovery, State Key Laboratory of Natural Medicine, China Pharmaceutical University, Nanjing 211198, China
[c] Department of Pharmacy, Fujian Medical University Union Hospital, Fuzhou 350001, China
* Corresponding author: Wancai Que (wancaique@fjmu.edu.cn); Yueqin Zheng (yzheng@cpu.edu.cn); Weiwei Guo (guoweiwei@cpu.edu.cn)

1. Experimental Section

1.1 Materials

Zinc acetate dihydrate ($Zn(OAc)_2 \cdot 2H_2O$), nickel acetate tetrahydrate ($Ni(OAc)_2 \cdot 4H_2O$), hydrazine hydrate (80%), 2-cyanopyrazole, di-tert-butyl dicarbonate, trifluoroacetic acid, L-arginine, 9,10-Anthraquinonylidenebis(methylene)-dicarboxylic acid (ABDA), and Nitro blue tetrazolium chloride (NBT) were obtained from Aladdin (Shanghai, China). Additional reagents included 8-anilino-1-naphthalenesulfonic acid (ANS), MTT, L-Arg Assay Kit, Reactive Oxygen Detection Kit (DCFH-DA), Nitric Oxide Assay Kit, NO fluorescent probe (DAF-FM DA), protease-phosphatase inhibitor mixture, crystal violet staining solution, LIVE/DEAD Cell Viability Assay Kit, SYTO-9 Live/Dead Bacteria Dual Staining Kit, 2.5% glutaraldehyde fixative, and streptozotocin (STZ), all purchased from Solarbio (Beijing, China). DMEM medium and fetal bovine serum (FBS) were obtained from Tianhang Biotechnology (Zhejiang, China), along with superoxide dismutase (SOD) and catalase (CAT) assay kits, malondialdehyde (MDA) detection kits, bacterial protein extraction kits, and o-nitrophenyl-β-D-galactopyranoside (ONPG). Mouse IL-6, IL-10, IL-1β, TNF-α, and MCP-1 ELISA kits were also supplied by liankebio (Zhejiang, China).

1.2 Methods

The morphological and structural properties of Zn-TDP, Ni-TDP, A@Zn-TDP, and A@Ni-TDP nanoparticles were analyzed using transmission electron microscopy (TEM, FEI Talos F200X G2, USA) and scanning electron microscopy (SEM, Hitachi Regulus 8100, Japan). Elemental distribution was determined through energy-dispersive X-ray (EDX) mapping using the TEM system. Crystal structures were examined with an X-ray powder diffractometer (Rigaku SmartLab SE, Japan), while chemical compositions were assessed via X-ray photoelectron spectroscopy (XPS, Thermo Scientific K-Alpha, USA). Fourier transform infrared spectroscopy (FT-IR, Tensor 27, Germany) was used to analyze the chemical structures of Zn-TDP, Ni-TDP, A@Zn-TDP, and A@Ni-TDP, and thermal stability was evaluated using a thermogravimetric analyzer (TGA 4000, PerkinElmer, USA). UV-visible absorption spectra were recorded using a Shimadzu UV-3600 spectrophotometer (Japan), and fluorescence measurements were carried out with a SpectraMax spectrometer (Thermo, USA). Bacterial and intracellular fluorescence were observed using a confocal laser scanning microscope (CLSM, FV3000, Olympus, Japan) and fluorescence inverted microscopy. Electron spin resonance (ESR) measurements were conducted using a Bruker EMXPlus spectrometer (Germany). All experiments were performed under a xenon lamp (Sunlight Analog Filter AM1.5, Beijing Magnesium Richen Technology Co., China) as the light source.

1.3 Synthesis of 1,4-dipyrazolotetrazine (H_2TDP) and 1,4-dipyrazolylbenzene (H_2BDP)

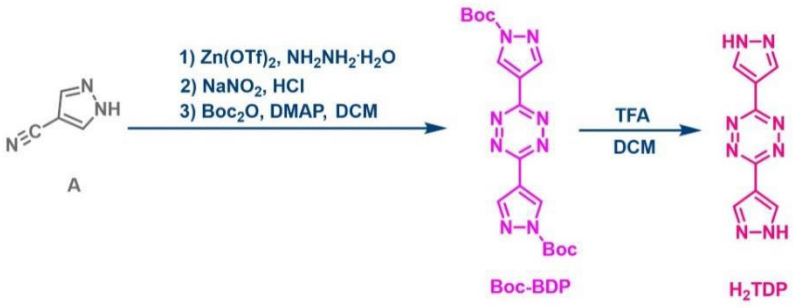

Figure S1. The synthesis procedure of linker H_2TDP.[1]

4-Cyanopyrazole (1.00 g, 10.74 mmol) and zinc trifluoromethanesulfonate (0.78 g, 2.14 mmol) were dispersed in 80% hydrazine hydrate (5.21 mL) and reacted under nitrogen at 60°C for 20 hours. After cooling to room temperature, the mixture was filtered, and the filtrate was collected. An aqueous sodium nitrite solution (5.93 g, 85.92 mmol) was added to the filtrate, and the pH was adjusted to 2–3 using 1 M hydrochloric acid, followed by stirring at room temperature for 6 hours. The resulting solution was filtered, and the filtrate was sequentially washed with water, methanol, and dichloromethane to yield the crude 1,4-dipyrazolium oxidized tetrazine product.

The crude product was then dispersed in dichloromethane, and di-tert-butyl dicarbonate (16.11 mmol) was added. The mixture was stirred at room temperature for 30 minutes. After removing the solvent, the residue was purified by flash column chromatography on silica gel (petroleum ether: ethyl acetate = 3 : 1), yielding compound B (3.21 g, 7.73 mmol) in 72% yield.

Compound B was dissolved in 20 mL of dichloromethane, and 4 mL of trifluoroacetic acid was added. The mixture was stirred at room temperature for 8 hours, then filtered, and the precipitate was washed with dichloromethane. The solid was transferred to a beaker containing 100 mL of distilled water, and the pH was adjusted to 6–7 using a 0.25 mM sodium hydroxide solution. The solid was filtered again, washed to neutrality with distilled water, and then rinsed with small amounts of ethanol and dichloromethane, yielding a pink solid (6.26 mmol) with an 81% yield. ^{1}H NMR (400 MHz, d6-DMSO) δ =8.53 (4H, s). HRMS: m/z: 213.0636 $[M-H]^-$.

1,4-Dipyrazolylbenzene (H_2BDP) was synthesized via Suzuki coupling, following established procedures in the literature. ^{1}H NMR (400 MHz, d6-DMSO) δ =7.58 (2H, s), 8.06(2H, s).

1.4 Electrochemical Measurements

The MOF (10 mg) was ground and mixed with 100 μL ethanol and 10 μL Nafion (5.0 wt%) and sonicated for 30 min to yield a dispersed suspension. This suspension was then coated onto fluorine-doped tin oxide (FTO) glass, scraped into a uniform film, and dried in oven for 2 h. Electrochemical measurements were conducted using a CHI-

760E workstation with the MOF-coated FTO as the working electrode, Pt wire as the counter electrode, and Ag/AgCl as the reference electrode. Visible light was simulated using a 150 mW/cm^2 Xe lamp with a UV cutoff filter ($\lambda \geq 420$ nm) for photocurrent measurements. Photo-responsive signals were recorded at 0.40 V in 0.50 M Na_2SO_4 solution, and Mott-Schottky plots were generated at 1000, 2000, and 3000 Hz. Electrochemical impedance spectroscopy (EIS) was performed in 0.50 M Na_2SO_4 solution with a sinusoidal wave of 5.0 mV over a frequency range of 100 kHz to 0.05 Hz.

1.5 Detection of ROS and NO

Photocatalytic Generation of Reactive Oxygen Species (ROS): The ability of Zn-TDP and Ni-TDP nanoenzymes to produce ROS, specifically singlet oxygen ($^1O_2$) and superoxide anion ($O_2^{\bullet-}$), was evaluated using EPR spectroscopy. Aqueous or methanol suspensions (2 mg/mL) of Zn-TDP and Ni-TDP were sonicated for 10 minutes in the dark. Spin probes, 5,5-dimethyl-1-pyrroline-N-oxide (DMPO) and 2,2,6,6-tetramethyl-1-piperidine (TEMP), were then added to the respective samples, followed by 10 minutes of light irradiation (400–470 nm). After irradiation, samples were immediately analyzed by EPR.

To quantify ROS, we used DCFH-DA as the detection agent. A solution of DCFH-DA in DMSO was treated with 0.01 M NaOH and incubated for 30 minutes at room temperature, protected from light. The reaction was halted by adding phosphate-buffered saline (PBS, pH 7), yielding a final DCFH concentration of 10 μM. Experimental groups included L-arginine, Zn-BDP, Zn-TDP, A@Zn-TDP, Ni-BDP, Ni-TDP, and A@Ni-TDP (each at 200 μg/mL) mixed with DCFH-DA, while DCFH-DA alone served as the control. Changes in absorbance (500–600 nm) were measured under dark conditions or xenon lamp irradiation (420–780 nm, 150 mW·cm^{-2}, 5min) to assess total ROS production.

Specific ROS Detection: For superoxide detection, nanoenzyme (100 μg/mL) samples were mixed with NBT (100 μg/mL) and irradiated with visible light. Samples were collected at 10-minute intervals, and the decrease in NBT absorbance at 259 nm

was recorded using a UV-Vis spectrophotometer. To quantify $^1O_2$, samples were mixed with 9,10-anthracenediyl-bis(methylene)dimalonic acid (ABDA), irradiated, and sampled every 5 minutes. The supernatant was diluted 2-fold in PBS and analyzed for absorbance decrease at 400 nm using a UV-Vis spectrophotometer.

Nitric Oxide Release: The release of NO from A@Zn-TDP and A@Ni-TDP was evaluated using a Griess Reagent Nitric Oxide Detection Kit during 60 minutes of visible light irradiation.

Glutathione Oxidation Assay: Glutathione (GSH) oxidizability was assessed using Ellman's reagent (DTNB). A 50 mM DTNB solution in PBS was prepared, and each nanoenzyme sample (Zn-BDP, Zn-TDP, A@Zn-TDP, Ni-BDP, Ni-TDP, and A@Ni-TDP) was mixed with GSH (0.4 mM) at a concentration of 200 μg/mL. The mixtures were exposed to visible light (150 $mW \cdot cm^{-2}$) and sampled at 10-minute intervals. After irradiation, DTNB (100 mM) was added to each sample for color development. The supernatant was centrifuged, and the absorbance was measured at 410 nm.

1.6 In Vitro Antimicrobial Activity

Concentration and Duration-Dependent Studies: Bacterial suspensions (10^8 CFU/mL) were treated with increasing concentrations of Zn-TDP (5, 15, 25, 50, 100 μg/mL), A@Zn-TDP (5, 15, 25, 50, 100 μg/mL), and A@Ni-TDP (50, 100, 150, 200, 250, 300 μg/mL) for 3 hours. After treatment, samples were exposed to light (420–780 nm, 150 $mW \cdot cm^{-2}$, 15 minutes for Zn-based and 30 minutes for Ni-based MOFs). Colony counts were performed post-irradiation. Further experiments were conducted using fixed concentrations (MRSA: A@Zn-TDP (25 μg/mL), A@Ni-TDP (250 μg/mL); *E. coli*: A@Zn-TDP (50 μg/mL), A@Ni-TDP (200 μg/mL); *S. aureus*: A@Zn-TDP (25 μg/mL), A@Ni-TDP (200 μg/mL)). Colony counts were recorded at varying durations (0, 5, 10, 15, 20, 30, and 40 minutes) and light intensities (0, 50, 100, 150, and 200 $mW \cdot cm^{-2}$).

Bacterial Growth Curves: For growth curve analysis, MRSA was co-incubated with saline, A@Zn-TDP (25 μg/mL), or A@Ni-TDP (250 μg/mL) at 37°C in the dark

for 3 hours. *E. coli* was treated with saline, A@Zn-TDP (50 μg/mL), or A@Ni-TDP (200 μg/mL), and *S. aureus* was treated similarly. All samples were then exposed to dark or light conditions, diluted to 10^5 CFU/mL, and cultured in LB liquid medium. Optical density at 600 nm (OD600) was measured at 2-hour intervals using a microplate reader.

Live/Dead Bacterial Staining: Bacterial suspensions treated as described above were centrifuged at 8000 rpm for 5 minutes and stained using the SYTO-9 Live/Dead Bacteria Dual Staining Kit (BTN11-220950, Beijing Biolabs Technology Co., Ltd.). Fluorescence was observed using an Olympus FV3000 confocal microscope.

SEM: Bacterial cells were processed as previously described, centrifuged, and fixed in 2.5% glutaraldehyde at 4°C for 4 hours. Dehydration was performed using a graded ethanol series (30%, 50%, 70%, 80%, 90%, and 100%) for 15 minutes each. Samples were lyophilized and imaged using a Hitachi Regulus 8100 SEM to observe morphological changes.

1.7 Peroxidative damage to bacterial cell membranes

Experimental Groups and MDA Content Analysis: Five experimental groups were established: Control+D, A@Zn-TDP+D, A@Ni-TDP+D, A@Zn-TDP+L, and A@Ni-TDP+L. MRSA, *E. coli*, and *S. aureus* were treated according to these protocols, and malondialdehyde (MDA) content was measured using a malondialdehyde assay kit (BC0025, Beijing Solebo Technology Co., Ltd.).

Outer and Inner Membrane Permeability: The outer membrane permeability of *E. coli* was evaluated by diluting the bacterial suspension in saline (OD600 = 0.2) and adding 20 μM ANS. Fluorescence was recorded using an enzyme labeling instrument (excitation: 380 nm; emission: 450–600 nm) and visualized with an inverted fluorescence microscope. Inner membrane permeability changes in MRSA, *E. coli*, and *S. aureus* were assessed using ONPG. Bacterial suspensions (OD600 = 1.0) were centrifuged, and 100 μL of supernatant was incubated with 100 μL of 10 mM ONPG for 24 hours at room temperature. Absorbance was measured at 420 nm using a microplate reader.

ROS and NO Production Analysis: ROS and NO production in MRSA, *E. coli*, and *S. aureus* was assessed using DCFH-DA and DAF-FM DA fluorescent probes, respectively. Bacterial suspensions (OD600 = 0.25) were divided into Control + D, A@Zn-TDP + D, A@Ni-TDP + D, A@Zn-TDP + L, and A@Ni-TDP + L groups. After a 3-hour incubation, the samples were exposed to darkness or light for 10 minutes, and fluorescence was visualized using an Olympus FV3000 confocal microscope.

Bacterial Oxidative Stress Analysis: MRSA, *E. coli*, and *S. aureus* (OD600 = 1.0) were subjected to the same treatment groups. NADH oxidase (NOX) activity was quantified using the NADH Oxidase Activity Assay Kit (BC0630, Solepol), while catalase (CAT) activity and superoxide dismutase (SOD) activity were measured using the corresponding kits (BC0200 and BC0175, Soleba).

Bacterial DNA Damage Assessment: Bacterial suspensions (OD600 = 0.25) of MRSA, *E. coli*, and *S. aureus* were treated as described previously. Cells were collected, resuspended in PBS, and stained using a one-step TUNEL assay kit (C1086, Shanghai Biyuntian Bio-Technology Co., Ltd.). Fluorescence images were obtained using a confocal laser scanning microscope (CLSM).

1.8 Anti-biofilm Assay

Crystal Violet Staining: MRSA, *E. coli*, and *S. aureus* suspensions (2×10^8 CFU/mL) were added to 24-well plates (4 mL per well) and incubated at 37°C for 48 hours to form mature biofilms. After washing twice with saline, the biofilms were assigned to the following treatment groups: Control+D, A@Zn-TDP+D (50 μg/mL), A@Ni-TDP+D (250 μg/mL), A@Zn-TDP+L (50 μg/mL), and A@Ni-TDP+L (250 μg/mL). The samples were incubated at 37°C for 12 hours, followed by exposure to either dark conditions ("D") or visible light irradiation ("L") for 30 minutes. After treatment, the supernatant was removed, and the biofilms were washed twice, fixed with 1 mL of methanol for 1 hour, and then treated with an additional 200 μL of methanol for another hour. Next, the wells were drained, and 200 μL of crystal violet dye was added to each well and incubated for 30 minutes. After washing three times, 200 μL of 30% oxalic acid was added, followed by a 30-minute incubation. Digital

photographs were taken, and absorbance at 590 nm was measured. The treated biofilm was resuspended in 1 mL of saline, diluted 100-fold, and 10 μL of the dilution was plated onto agar. Bacterial colonies were counted after incubation at 37°C for 12 to 20 hours.

Biofilm Fluorescence Staining: Bacterial suspensions (2×10^8 CFU/mL) were added to confocal Petri dishes or 24-well plates and incubated at 37°C for 48 hours to promote biofilm formation. The biofilms were stained using the SYTO-9/PI Live/Dead Bacteria Dual Staining Kit (BTN11-220950, Beijing BioLite Technology Co., Ltd.) and visualized in 3D using an Olympus FV3000 confocal microscope. After washing and centrifugation, the biofilms were stained with SYTO-9 and PI solutions and incubated in the dark for 15 minutes. Fluorescence analysis was performed using a flow cytometer (FITC channel for SYTO-9, PE channel for PI).

SEM: Biofilm and bacterial morphology were analyzed using SEM. After treatment, the biofilms were fixed with 2.5% glutaraldehyde at 4°C for 4 hours, followed by dehydration in a graded ethanol series (30%, 50%, 70%, 80%, 90%, and 100%) for 15 minutes at each concentration. Samples were then lyophilized and imaged using a Hitachi Regulus 8100 SEM (Japan) for detailed morphological observation.

1.9 Biocompatibility Experiments

Cell Culture: Human umbilical vein endothelial cells (HUVECs) and human keratinocytes (HaCaT) were cultured in DMEM containing 10% fetal bovine serum (FBS) and antibiotics at 37°C in a humidified incubator with 5% CO_2.

MTT Assay: HUVECs and HaCaT cells were seeded in 96-well plates at a density of 8×10^3 cells per well. After 24 hours, the medium was replaced with fresh DMEM containing varying concentrations of A@Zn-TDP (0, 6.25, 12.5, 25, 50, 100 μg/mL) or A@Ni-TDP (0, 25, 50, 100, 150, 200, 250, 300 μg/mL). After another 24-hour incubation, 10 μL of MTT solution (5 mg/mL) was added to each well and incubated for 4 hours at 37°C. The medium was then removed, and 150 μL of DMSO was added to dissolve the resulting formazan crystals. Absorbance was measured at 570 nm using a microplate reader.

Live/Dead Cell Staining: After a 24-hour incubation, cells in 96-well plates were treated with fresh DMEM containing A@Zn-TDP (50 μg/mL) or A@Ni-TDP (250 μg/mL) for 24 or 48 hours. Cell viability was determined using the LIVE/DEAD staining kit (CA1630, Beijing Solepol Technology Co., Ltd.). Staining was performed at baseline, as well as at 24 and 48 hours post-treatment, and visualized using an inverted fluorescence microscope.

Hemolysis Assay: Red blood cells were collected from healthy ICR mice and diluted in PBS. Each sample (20 μL) was mixed with 1 mL of A@Zn-TDP or A@Ni-TDP at different concentrations (A@Zn-TDP: 0, 12.5, 25, 50, 75, 100, 150 μg/mL; A@Ni-TDP: 0, 50, 75, 100, 150, 200, 250, 300 μg/mL), along with ultrapure water and PBS as positive and negative controls. The mixtures were incubated at 37°C for 4 hours and centrifuged at 3000 rpm for 15 minutes. Hemoglobin release was measured by the absorbance of the supernatant at 540 nm using a microplate reader, with photographic documentation of the results.

1.10 Animal experimentation

Evaluation of Diabetic MRSA Biofilm-Infected Wound Healing: C57BL/6 mice (Yangzhou University's Comparative Medicine Center) were acclimated for one week, then fed a high-fat diet for four weeks. After an 18-hour fasting period, they received intraperitoneal injections of streptozotocin (STZ, 60 mg/kg) for four consecutive days. Mice with fasting blood glucose levels exceeding 11 mmol/L were classified as diabetic. Under isoflurane anesthesia, MRSA-infected wounds were created on the dorsal surface. Mice were randomly assigned to six groups (n = 6 per group): Control+D, A@Zn-TDP+D, A@Zn-TDP+L, A@Ni-TDP+D, A@Ni-TDP+L, and vancomycin.

Wound healing was monitored over 21 days, with assessments on days 1, 4, 7, 10, 14, and 21. Photographs were taken for documentation, and wound areas were measured using ImageJ software. Changes in body weight and blood glucose levels were recorded to monitor overall health. Mice were sacrificed on days 4 and 21, and wound tissues were collected for further analysis. On day 4, ELISA was used to

quantify inflammatory cytokines, and wound morphology was evaluated through H&E and Masson's trichrome staining. On day 21, the same assays were repeated to assess tissue architecture and inflammatory response.

2. Results

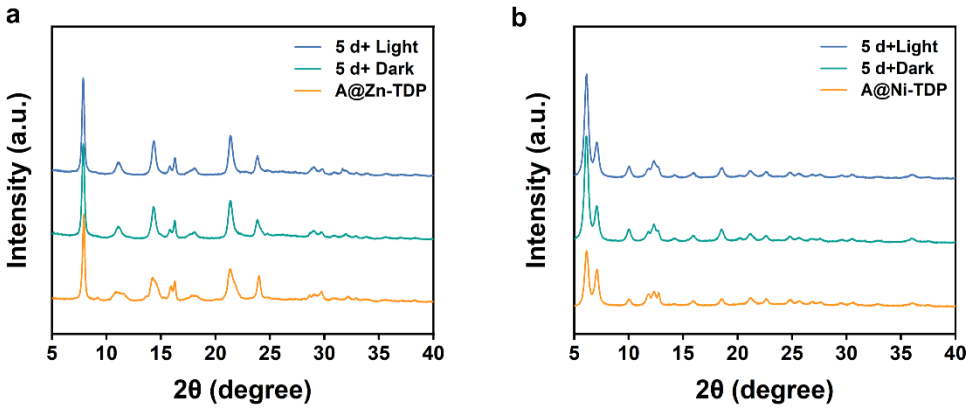

Figure S2. PXRD patterns of Zn-TDP (a) and Ni-TDP (b) after 5 d saline immersion under dark or light conditions, as well as A@Zn-TDP (a) and A@Ni-TDP (b).

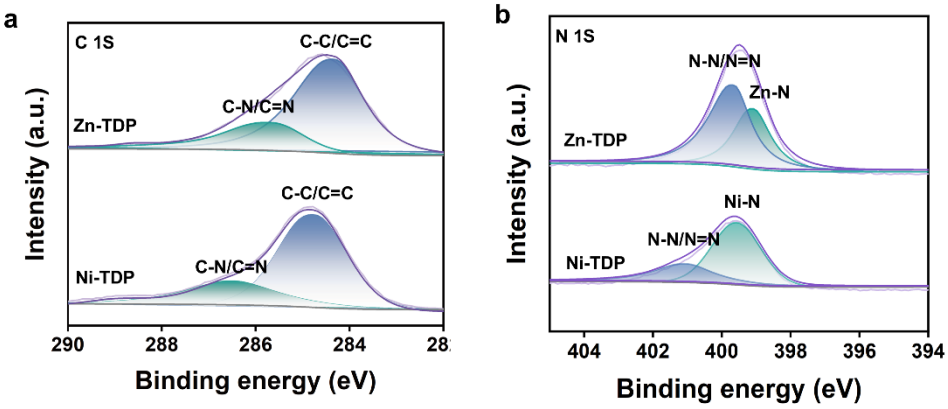

Figure S3. XPS spectra of Zn-TDP and Ni-TDP showing profile of C 2p (a) and N 2p (b).

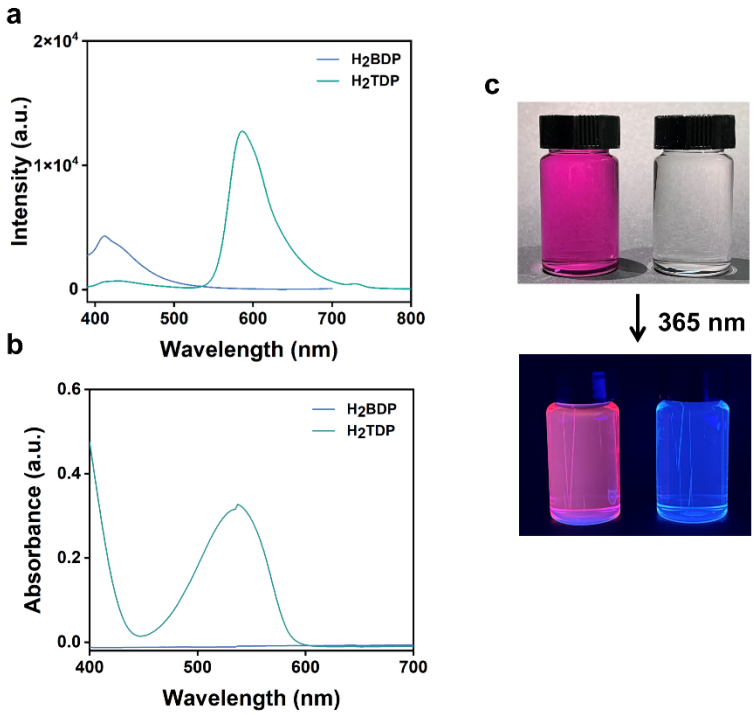

Figure S4. (a) Normalized luminescence spectra of H_2BDP and H_2TDP in DMF solution (λex = 365 nm). (b) UV-Vis absorption spectra of H_2BDP and H_2TDP in DMF solution. (c) Photographs of H_2BDP and H_2TDP in DMF solution under visible and 365 nm light excitation.

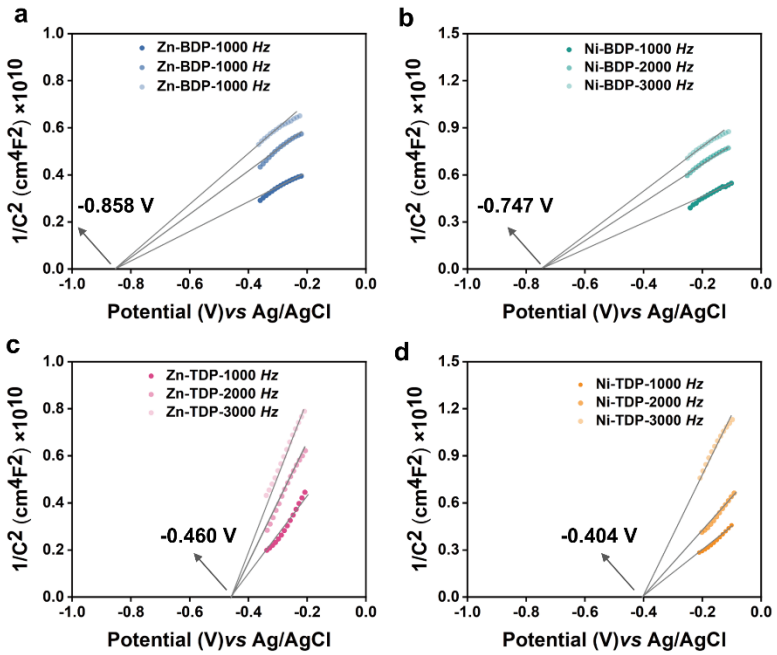

Figure S5. Mott-Schottky plots for Zn-BDP (a), Ni-BDP (b), Zn-TDP (c), and Ni-TDP (d).

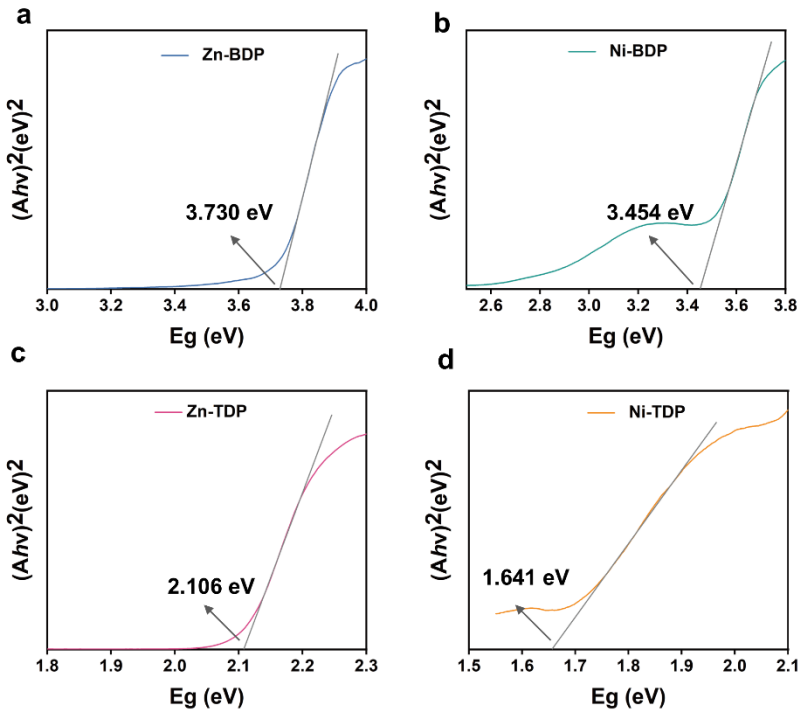

Figure S6. Tauc plots for Zn-BDP(a), Ni-BDP (b), Zn-TDP (c), and Ni-TDP (d).

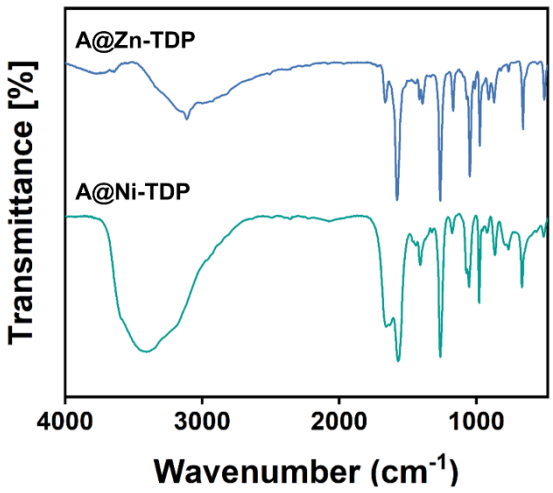

Figure S7. FT-IR spectra of A@Zn-TDP and A@Ni-TDP.

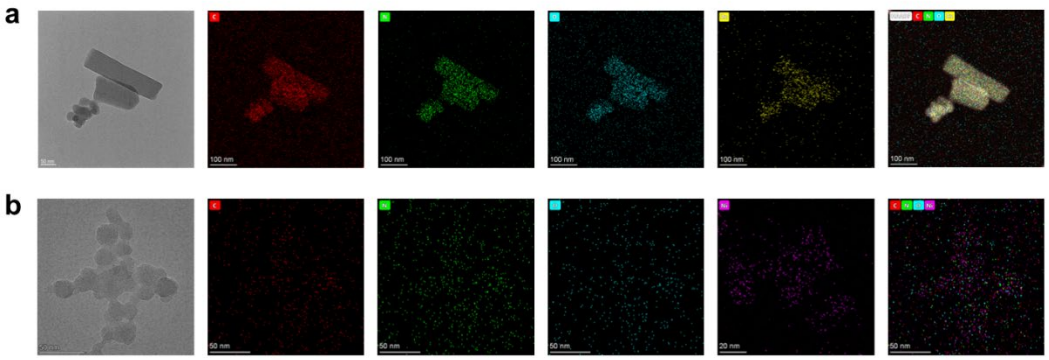

Figure S8. (a)TEM image of A@Zn-TDP and the EDS elemental mapping. (b) TEM image of A@Ni-TDP and the EDS elemental mapping.

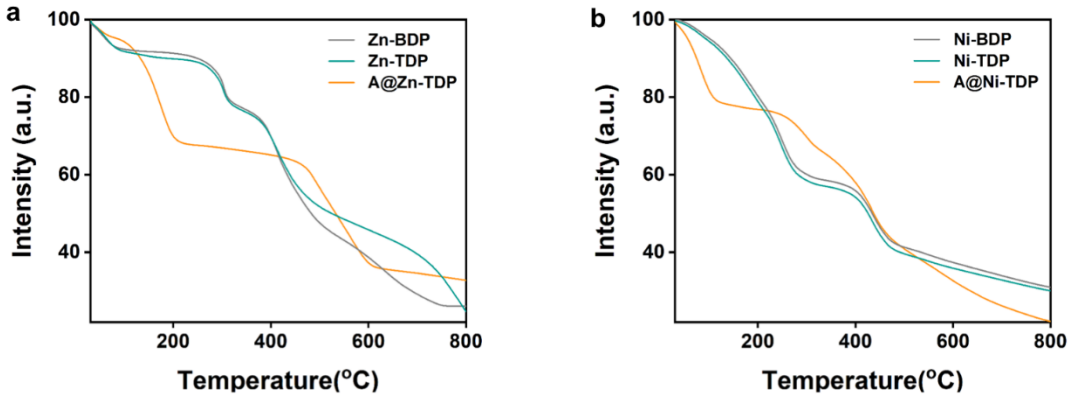

Figure S9. Thermogravimetric analysis for Zn-TDP, Zn-BDP, and A@Zn-TDP (a), and for Ni-TDP, Ni-BDP, and A@Ni-TDP (b).

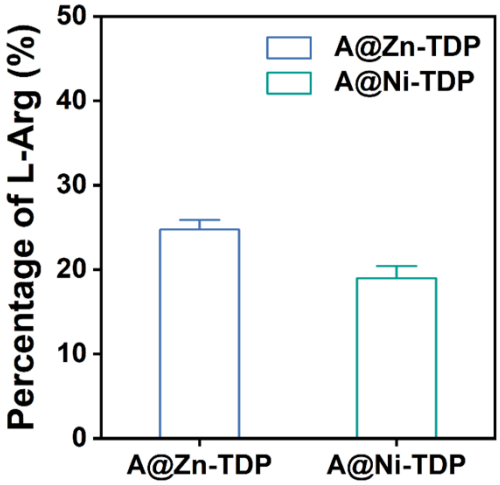

Figure S10. Statistical plots showing the loading of L-Arg in A@Zn-TDP and A@Ni-TDP.

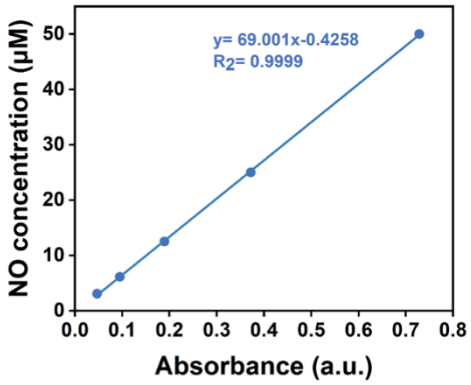

Figure S11. Standard curve of NO measured by NO assay kit.

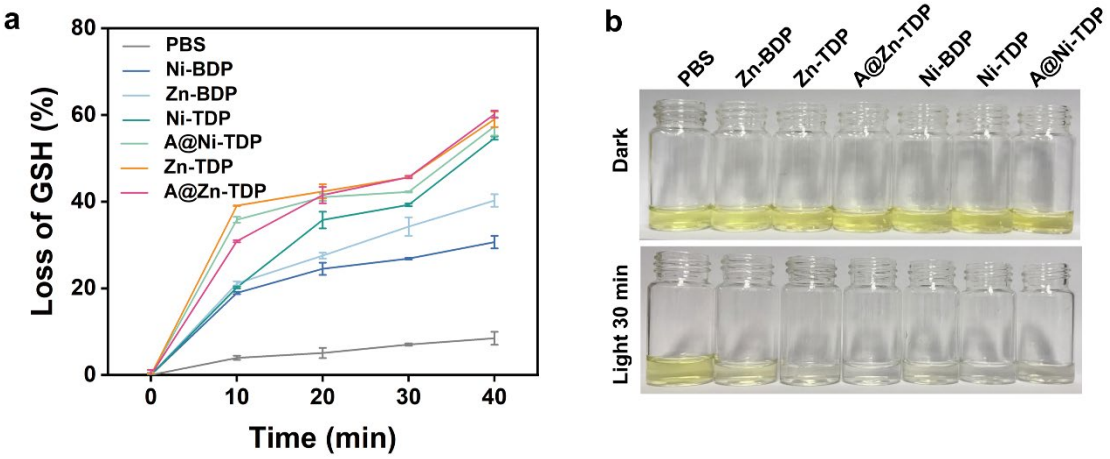

Figure S12. Irradiation time-dependent plot of the reduction of GSH (a) and photographs showing color changes (b).

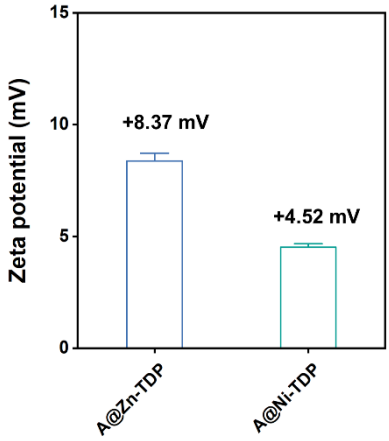

Figure S13. Zeta potential characterizations of A@Zn-TDP and A@Ni-TDP (n=3).

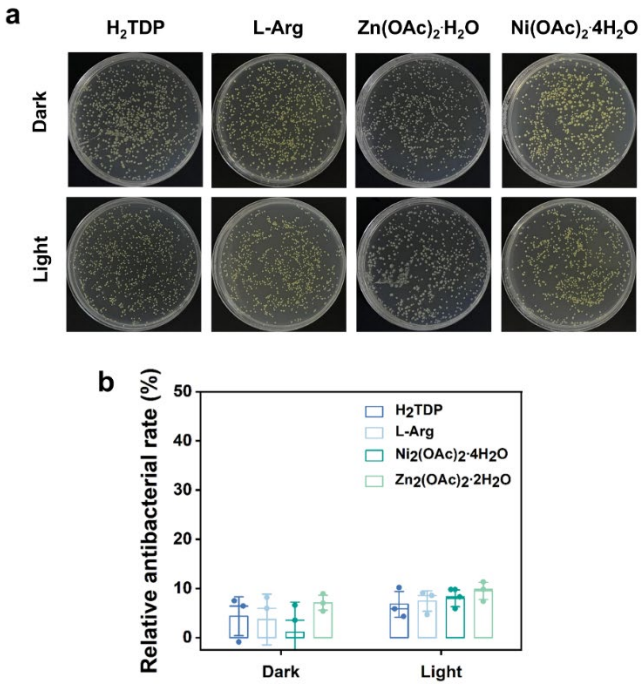

Figure S14. Plate coating (a) and the antimicrobial rates (b) of MRSA after dark and light treatments with H_2TDP, L-Arg, $Zn(OAc)_2.H_2O$, and $Ni(OAc)_2.4H_2O$.

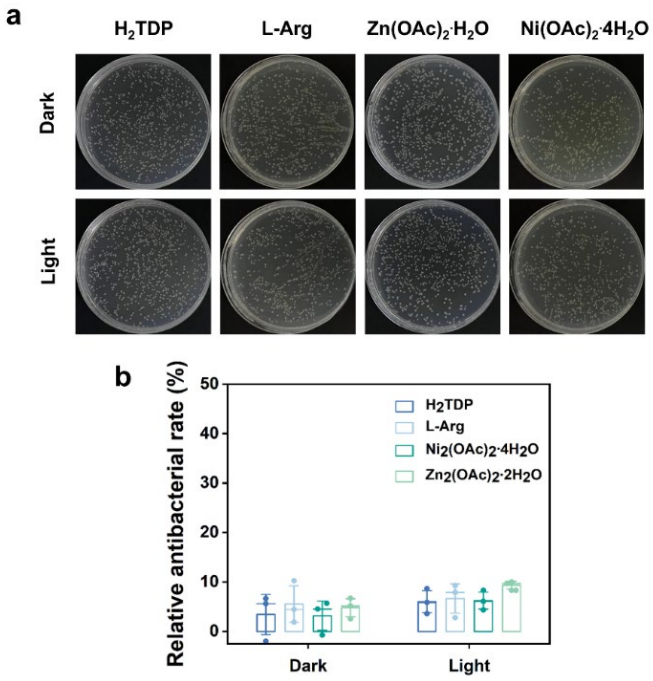

Figure S15. Plate coating (a) and the antimicrobial rates (b) of *E. coli* after dark and light treatments with H_2TDP, L-Arg, $Zn(OAc)_2.H_2O$, and $Ni(OAc)_2.4H_2O$.

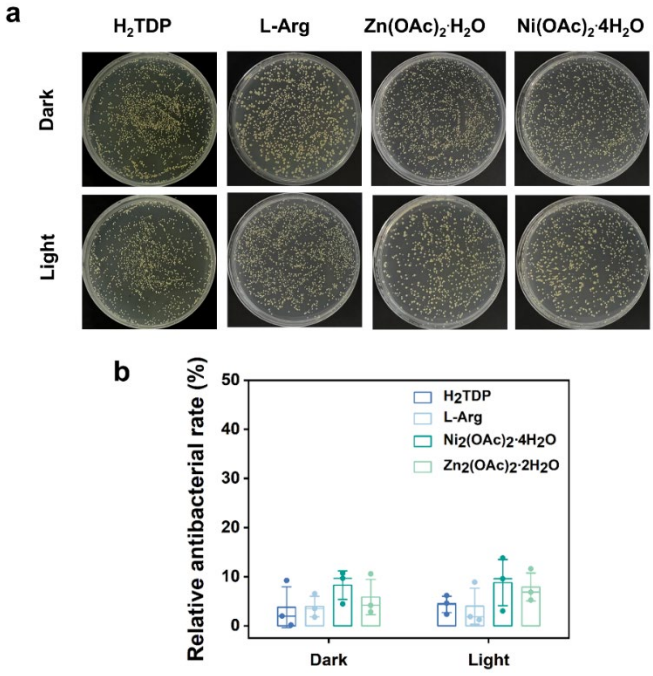

Figure S16. Plate coating (a) and the antimicrobial rates (b) of *S. aureus* after dark and light treatments with H_2TDP, L-Arg, $Zn(OAc)_2.H_2O$, and $Ni(OAc)_2.4H_2O$.

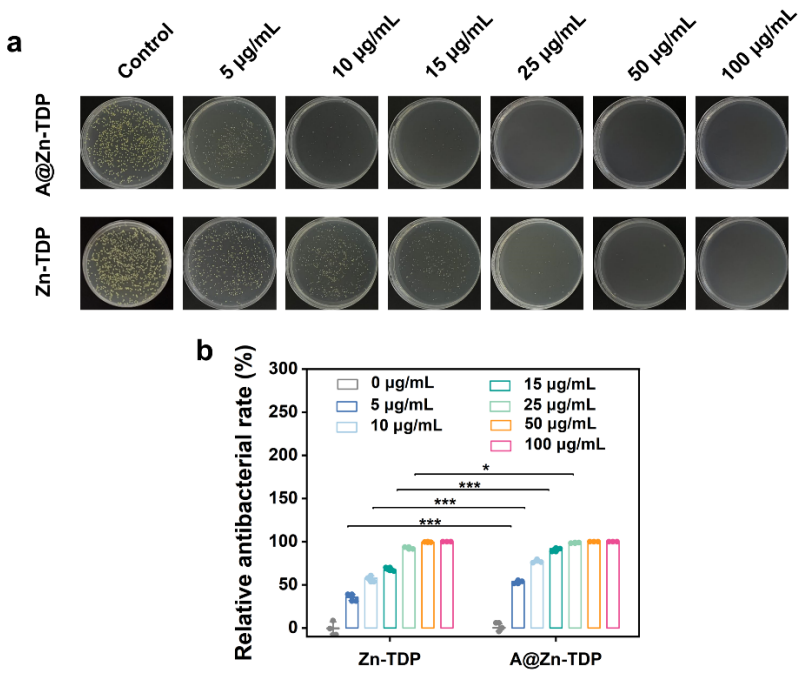

Figure S17. Plate coating (a) and the antimicrobial rates (b) of MRSA after light treatment with different concentrations of Zn-TDP and A@Zn-TDP.

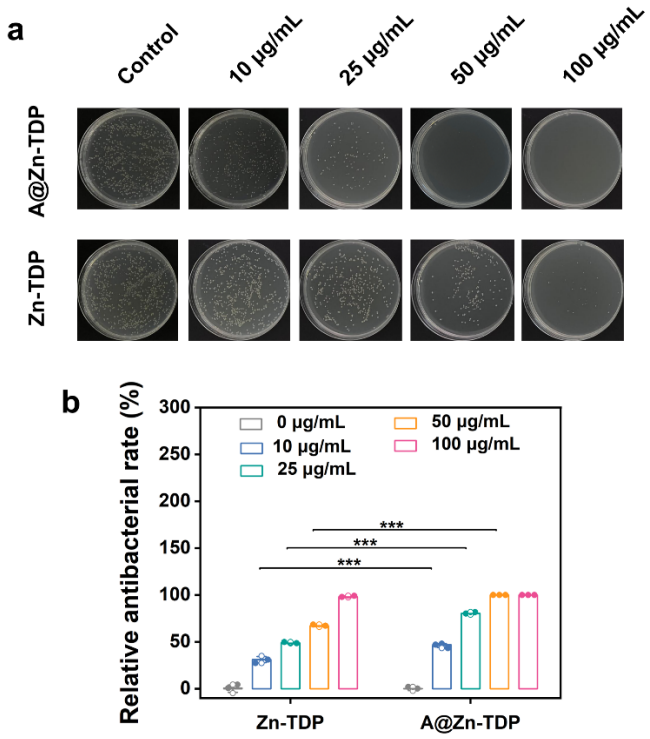

Figure S18. Plate coating (a) and the antimicrobial rates (b) of *E. coli* after light treatment with different concentrations of Zn-TDP and A@Zn-TDP.

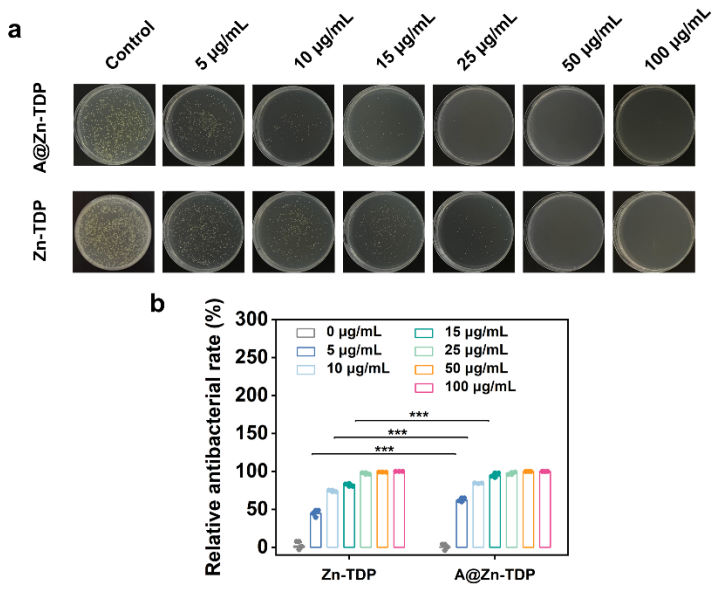

Figure S19. Plate coating (a) and the antimicrobial rates (b) of *S. aureus* after light treatment with different concentrations of Zn-TDP and A@Zn-TDP.

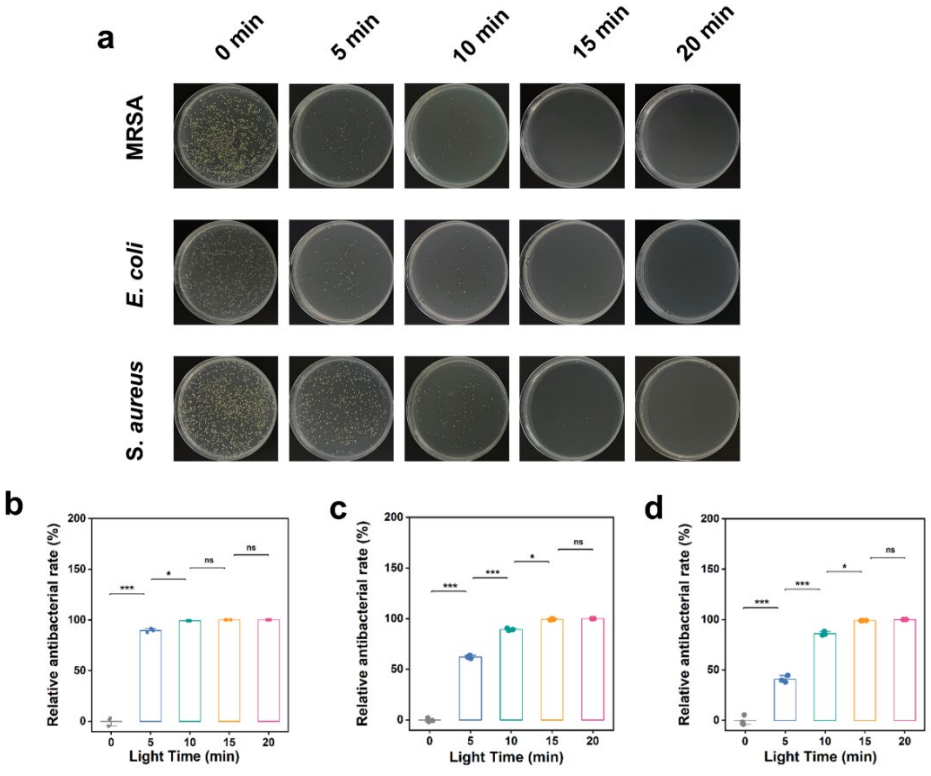

Figure S20. Co-incubation of MRSA, *E. coli* and *S. aureus* and A@Zn-TDP after treatment with different light times for plate coating (a) and the antimicrobial rates against MRSA (b), *E. coli* (c), and *S. aureus* (d).

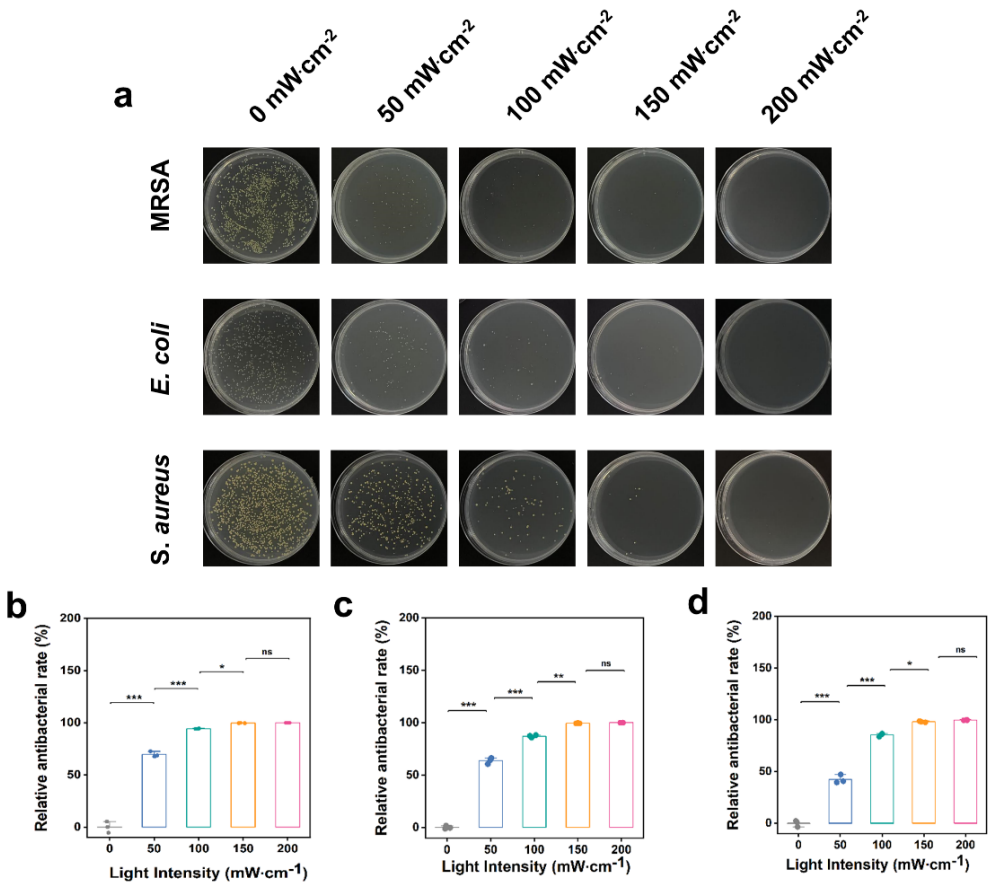

Figure S21. Co-incubation of MRSA, *E. coli*, *S. aureus* and A@Zn-TDP after visible light irradiation at different intensities for plate coating (a) and the antimicrobial rates against MRSA (b), *E. coli* (c), and *S. aureus* (d).

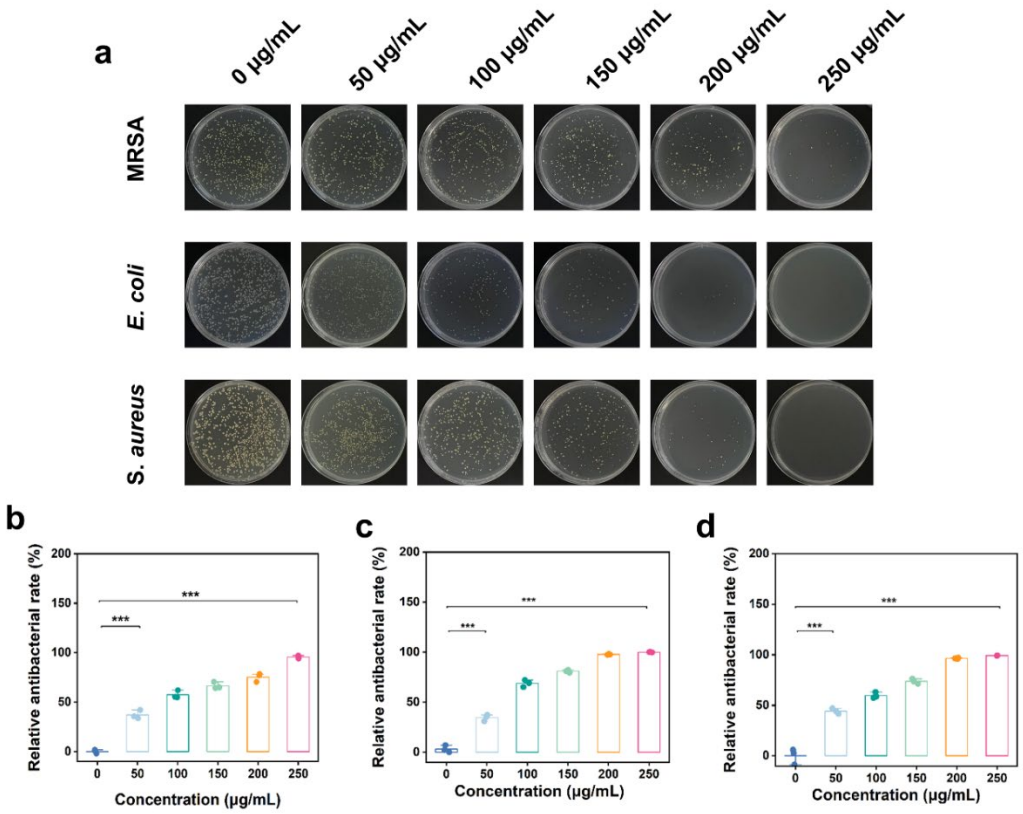

Figure S22. Plate coating of MRSA, *E. coli* and *S. aureus* after light treatment with different concentrations of A@Ni-TDP (a) and the antimicrobial rates against MRSA (b), *E. coli* (c) and *S. aureus* (d).

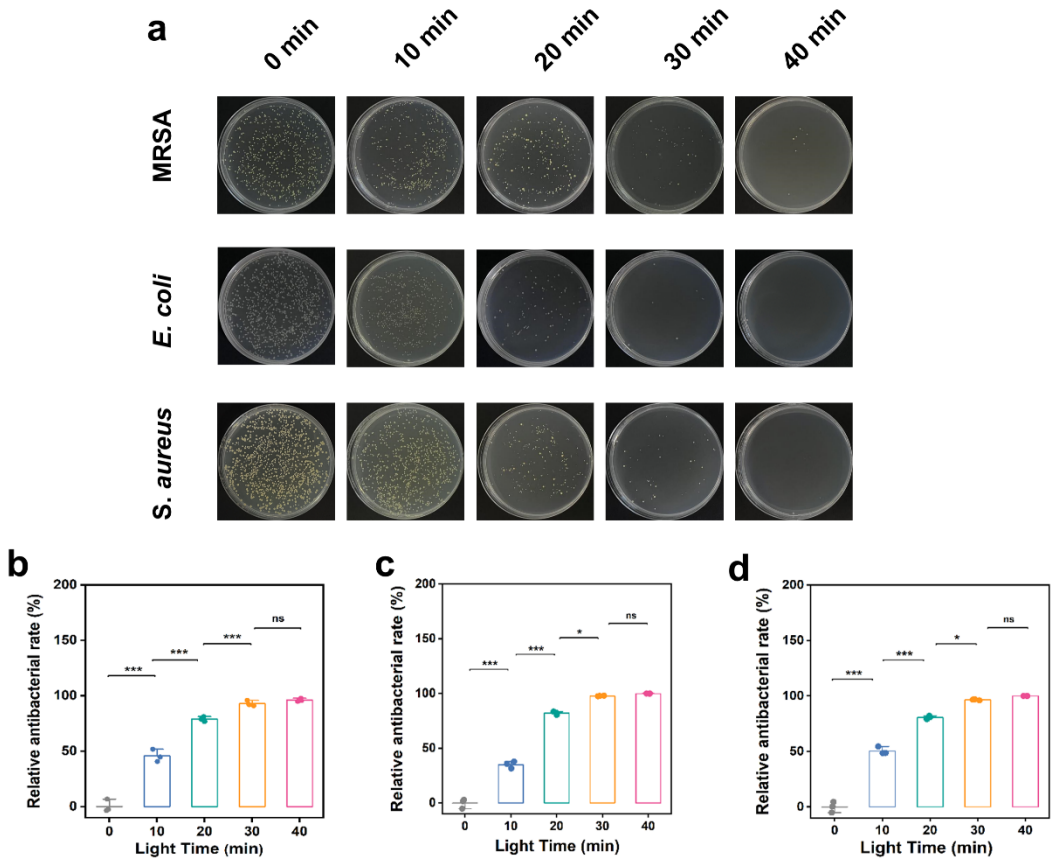

Figure S23. Plate coating of MRSA, *E. coli* and *S. aureus* and A@Ni-TDP after co-incubation by light for different times (a) and the antibacterial rate against MRSA (b), *E. coli* (c), and *S. aureus* (d).

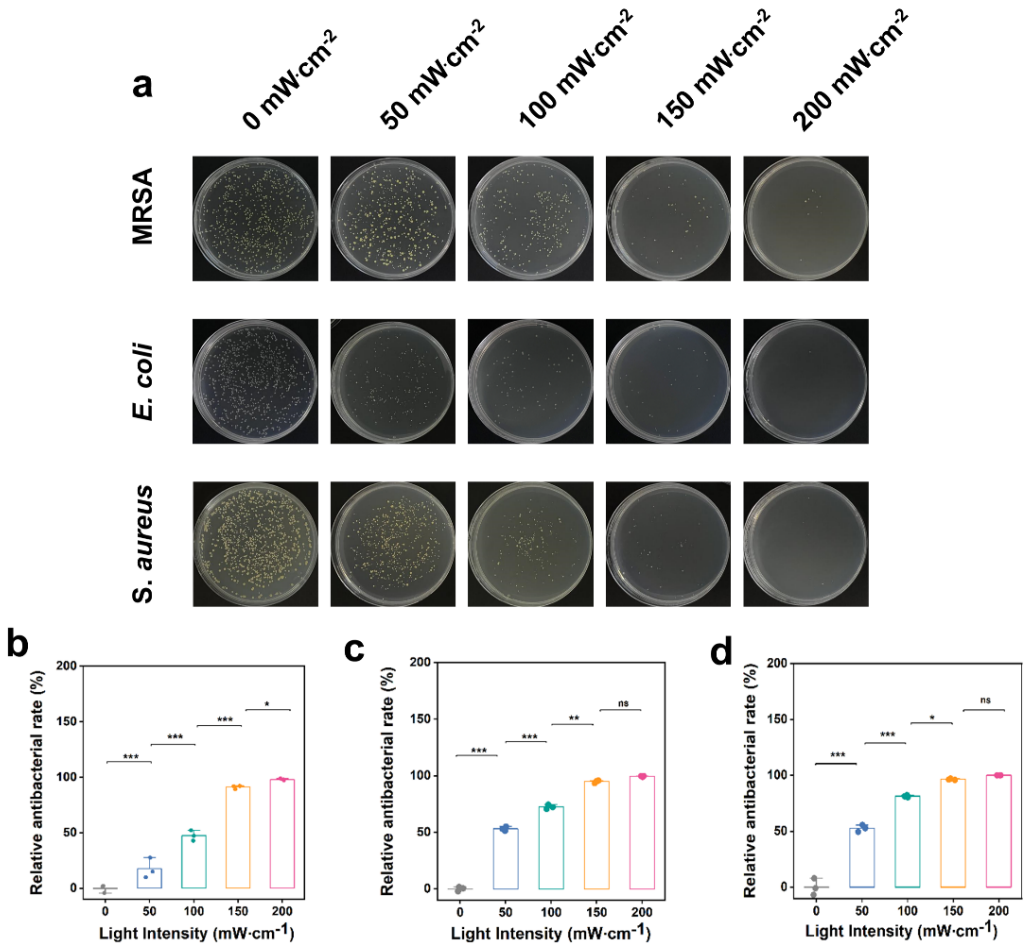

Figure S24. Co-incubation of MRSA, *E. coli*, *S. aureus* and A@Ni-TDP after irradiation with different intensities of visible light for plate coating (a) and the antimicrobial rates against MRSA (b), *E. coli* (c), and *S. aureus* (d).

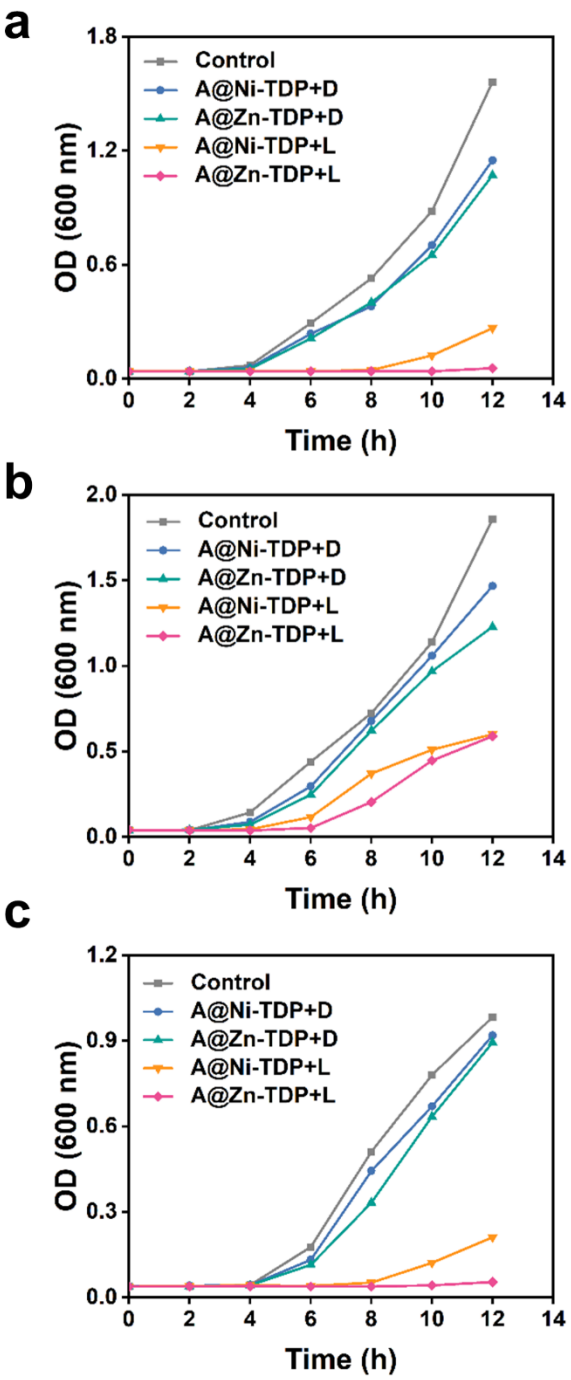

Figure S25. Growth curves of MRSA(a), *E. coli* (b), and *S. aureus* (c), after different treatments in LB liquid medium in a period of 12 hours.

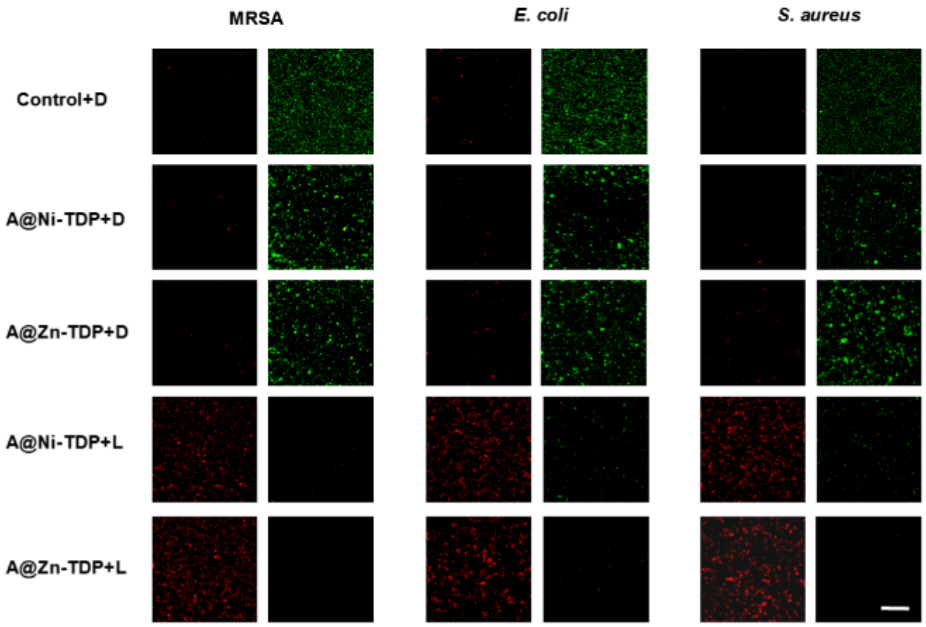

Figure S26. Fluorescence plots of SYTO-9/PI staining of MRSA, *E. coli* and *S. aureus* after different treatments, scale bar = 200 μm.

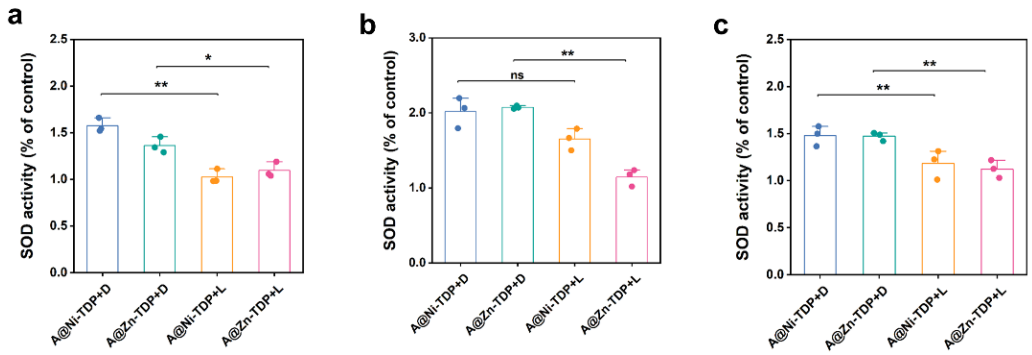

Figure S27. Levels of SOD oxidase activity in MRSA (a), *E. coli* (b) and *S. aureus* (c) after different treatments.

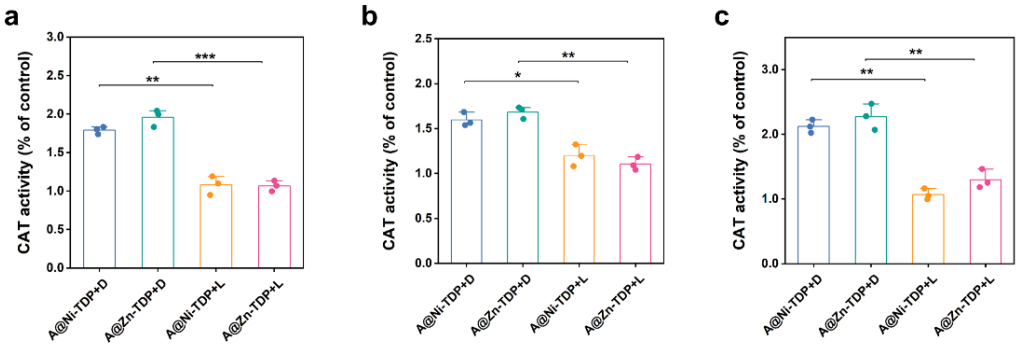

Figure S28. Levels of CAT oxidase activity in MRSA (a), *E. coli* (b) and *S. aureus* (c) after different treatments.

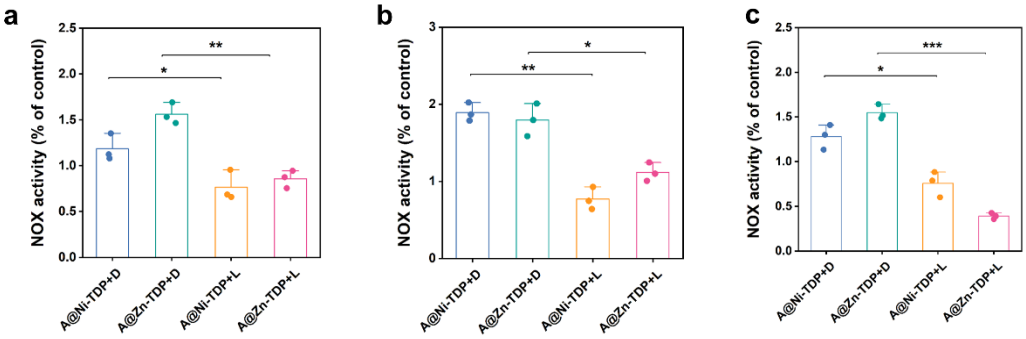

Figure S29. Levels of NOX oxidase activity in MRSA (a), *E. coli* (b) and *S. aureus* (c) after different treatments.

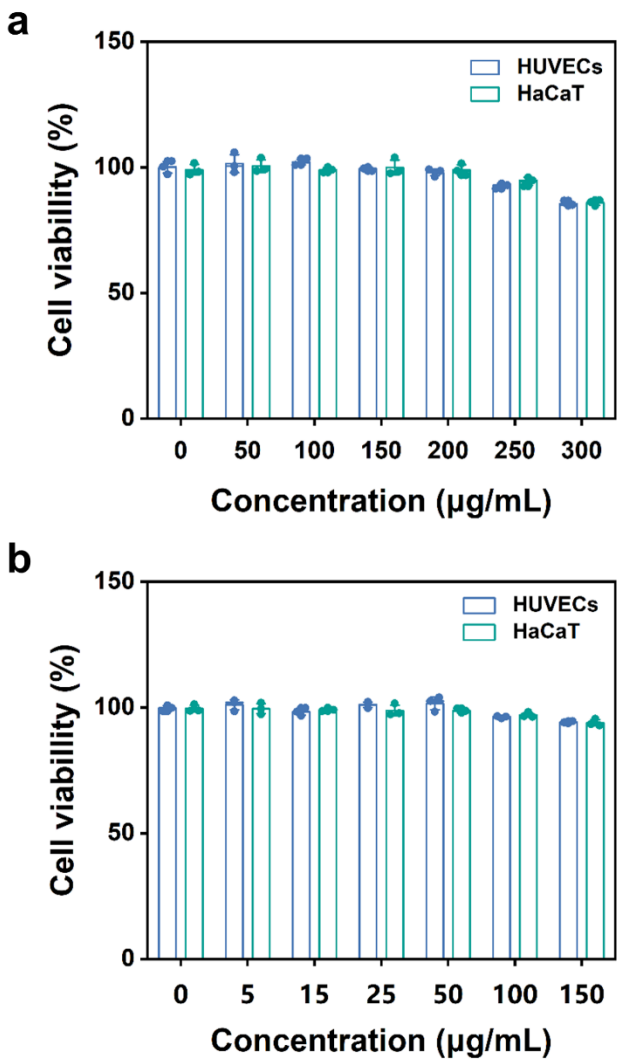

Figure S30. MTT assay to determine cell survival of HUVECs and HaCaT after 24 h of co-incubation with A@Ni-TDP (a) and A@Zn-TDP (b).

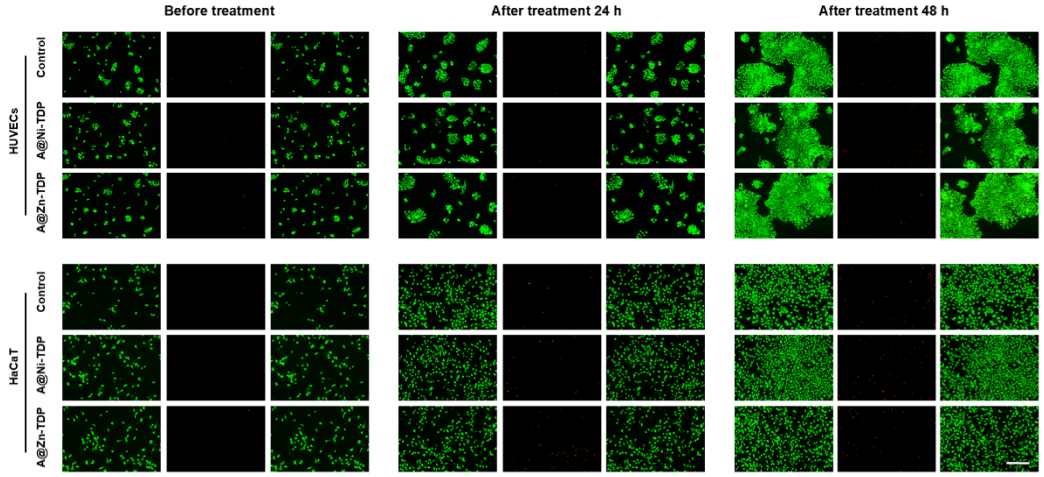

Figure S31. Fluorograms of live-dead cell staining after co-incubation of HUVECs and HaCaT cells with A@Zn-TDP and A@Ni-TDP for 24 h and 48 h. Scale bar = 200 μm.

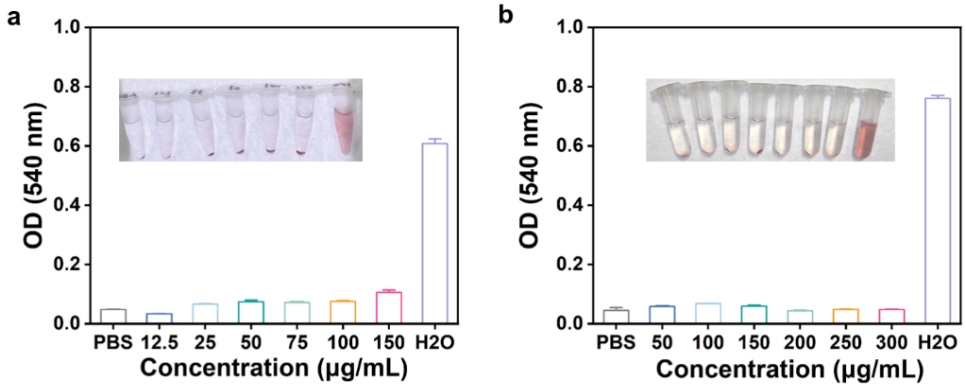

Figure S32. Hemolysis experiments of A@Zn-TDP (a) and A@Ni-TDP (b).

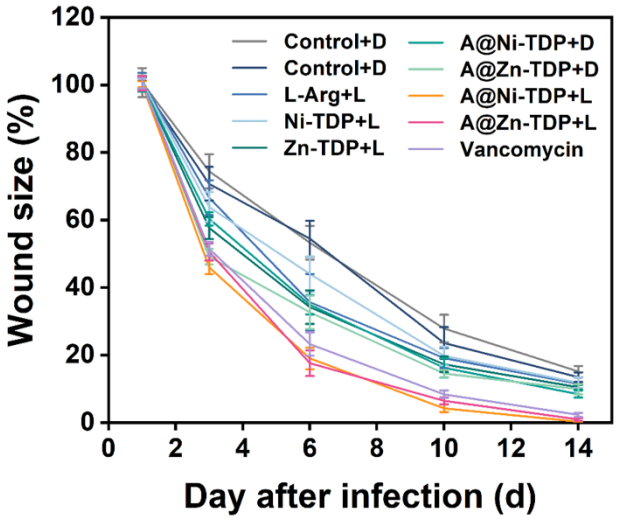

Figure S33. Statistical analysis of wound healing rates over a 14-day period for common infected wounds.

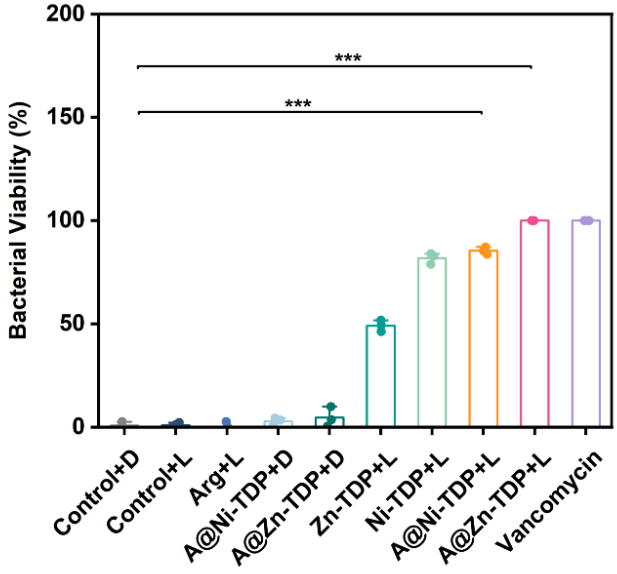

Figure S34. Mortality rate of MRSA calculated from tissue fluid plate smears at the wound site on day 2 after different treatments for common infected wounds.

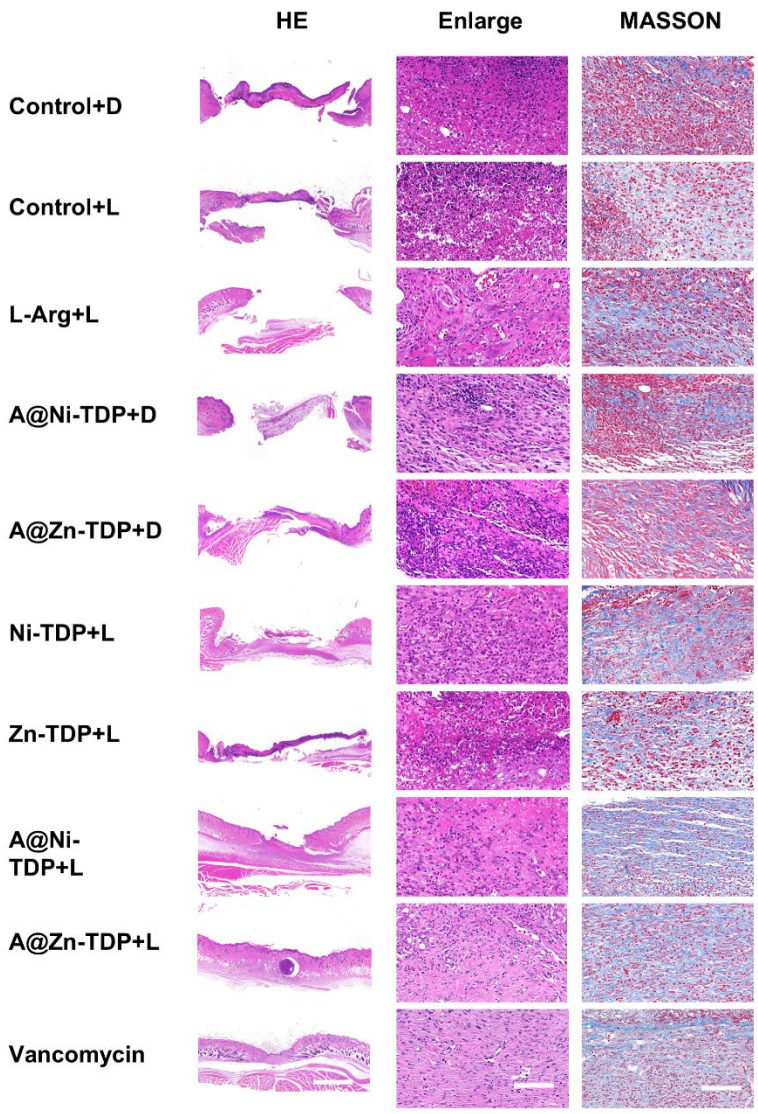

Figure S35. H&E and MASSON staining of wound tissue of common infected wounds on day 4 after different treatments, scale bar = 1000 μM (HE), scale bar = 50 μM (Enlarge and MASSON）.

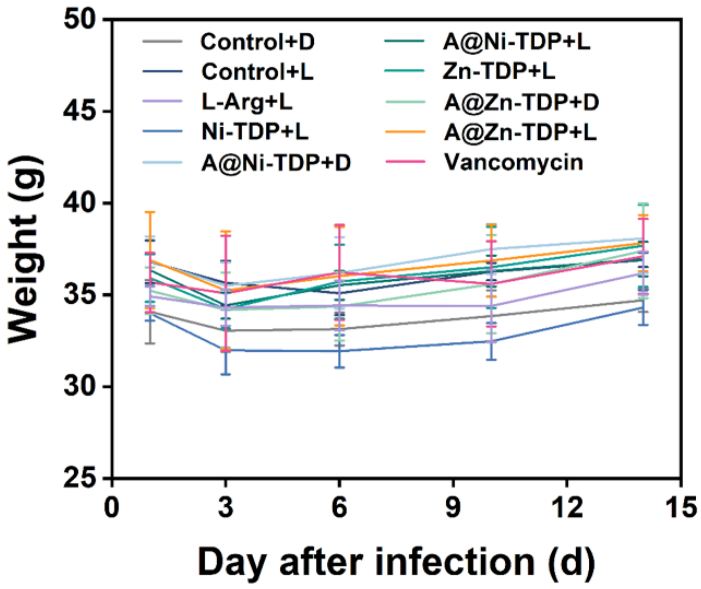

Figure S36. Changes in weight in common infected wounds in 14 days after different treatments.

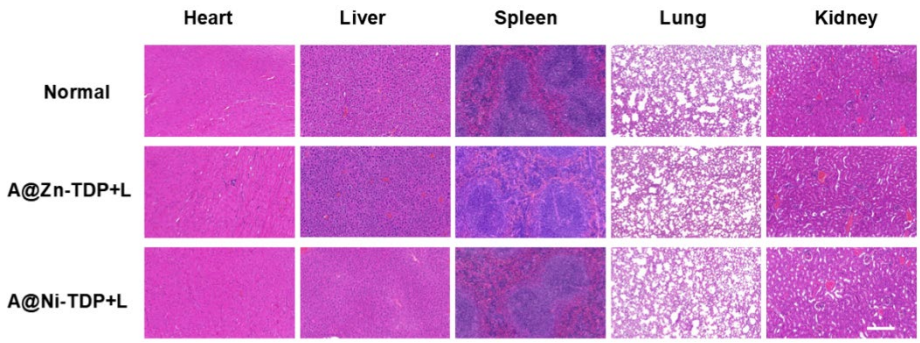

Figure S37. H&E staining of major organs (heart, liver, spleen, lungs, and kidneys) at day 14 after different treatments for common infected wounds, scale bar = 50 μM.

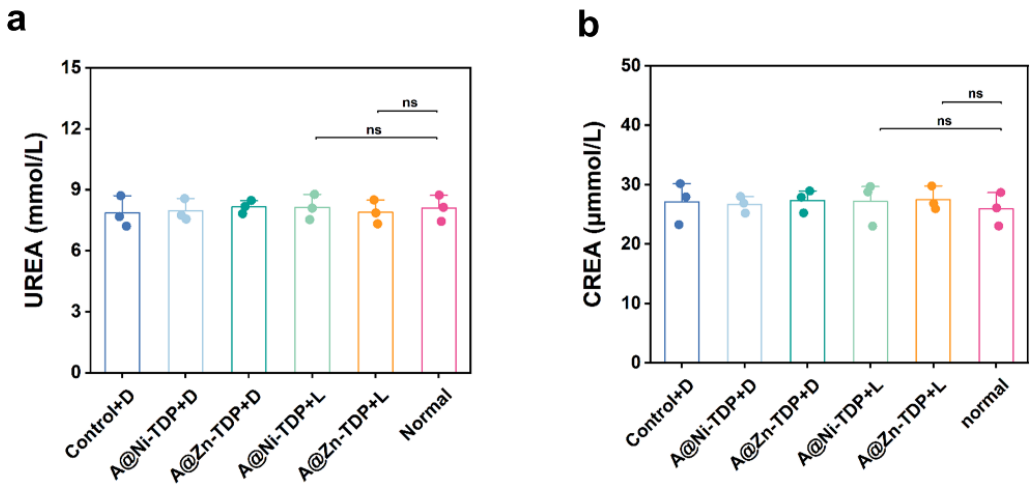

Figure S38. Serum UREA and CREA levels measured at day 14 after different treatments for common infected wounds.

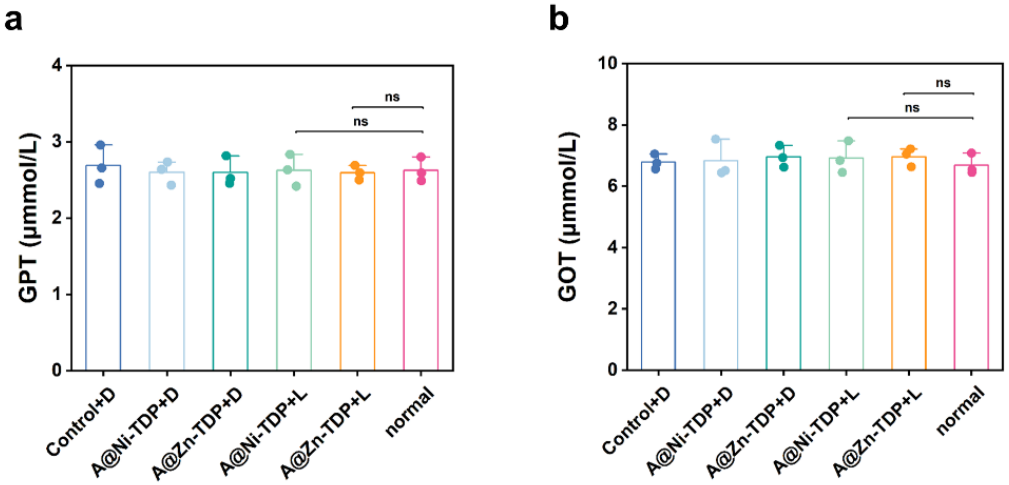

Figure S39. Serum GPT and GOT levels measured at day 14 after different treatments for common infected wounds.

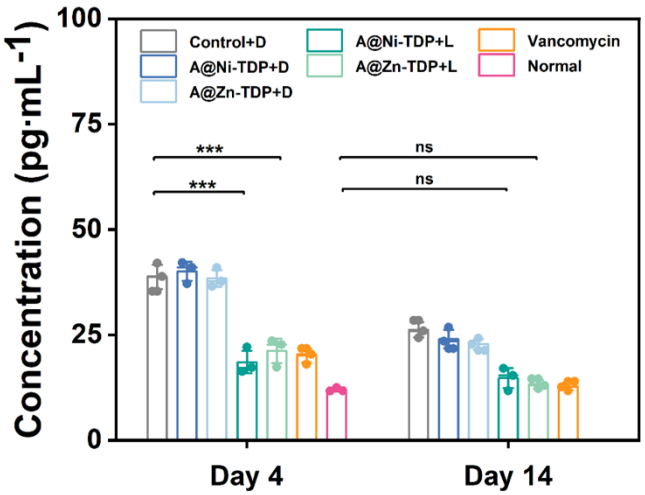

Figure S40. The TNF-α levels in wound tissue by ELISA for common infected trauma model.

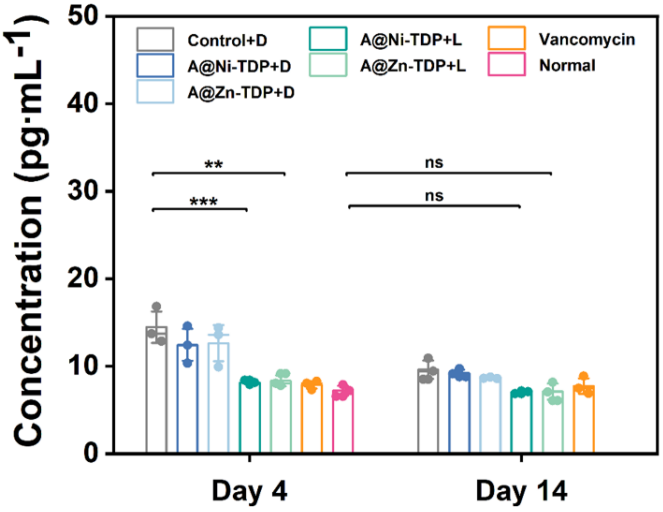

Figure S41. The MCP-1 levels in wound tissue by ELISA for common infected trauma model.

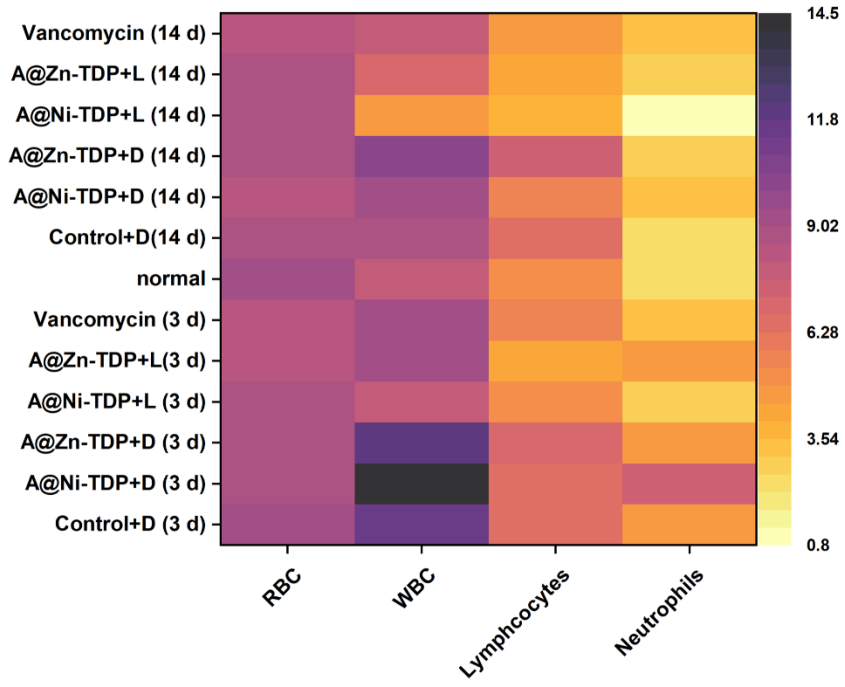

Figure S42. Whole blood analysis of common infected trauma model mice on day 4 after different treatments.

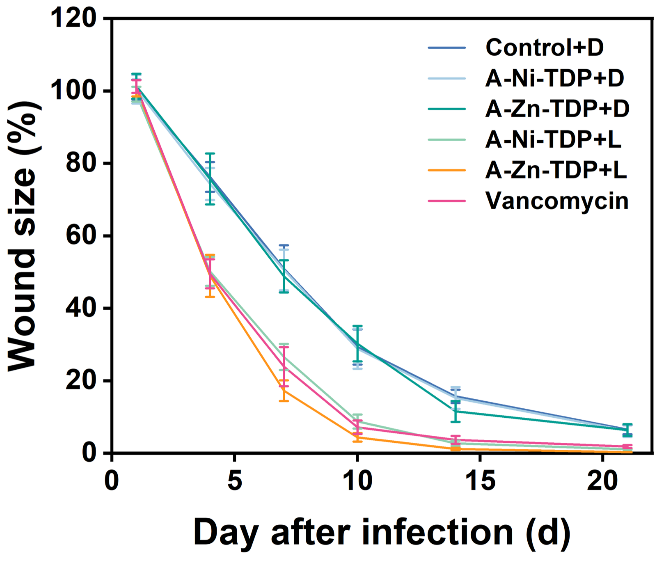

Figure S43. Statistical analysis of wound healing rates over a 21-day period for diabetic infected wounds.

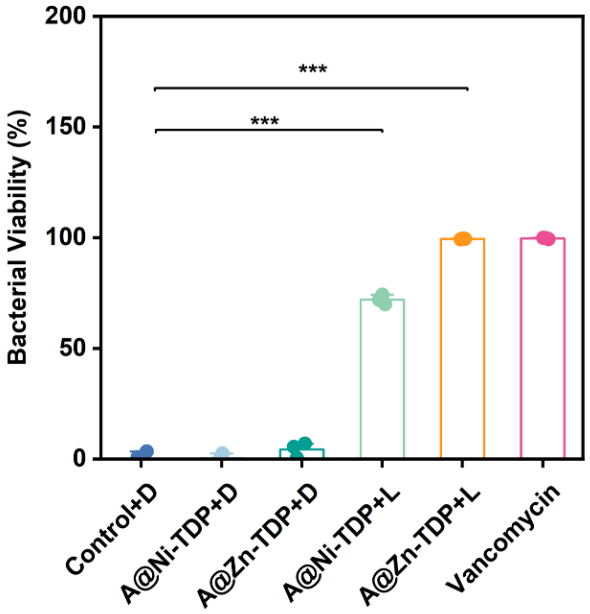

Figure S44. Tissue fluid plate smears at the wound site of diabetic infected wounds on day 2 after different treatments to calculate MRSA mortality.

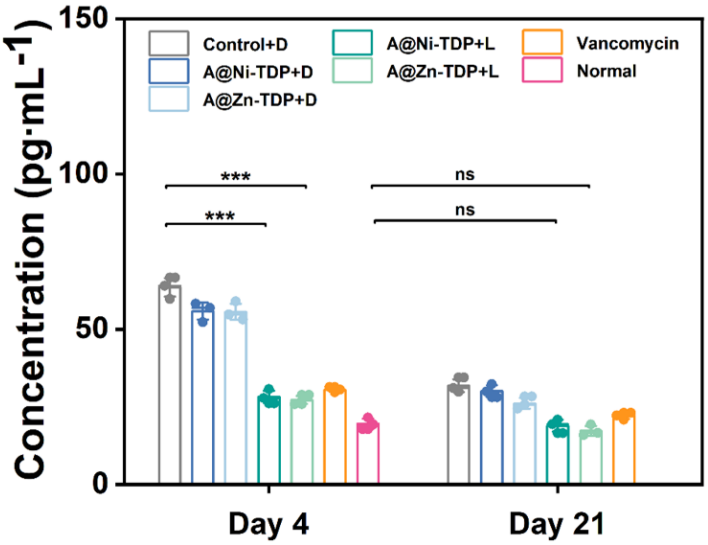

Figure S45. ELISA for the determination of IL-1β in wound tissue of diabetic infected wounds on day 4 and 21 after different treatments.

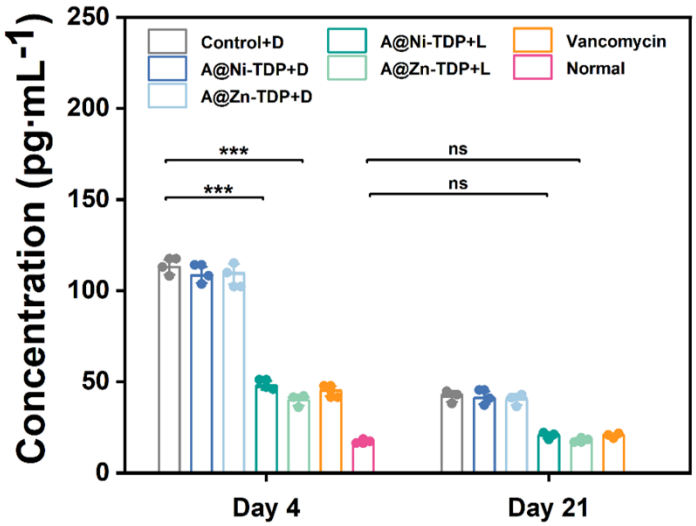

Figure S46. Determination of TNF-α in trabecular tissues of diabetic infected wounds by ELISA on day 4 and 21 after different treatments.

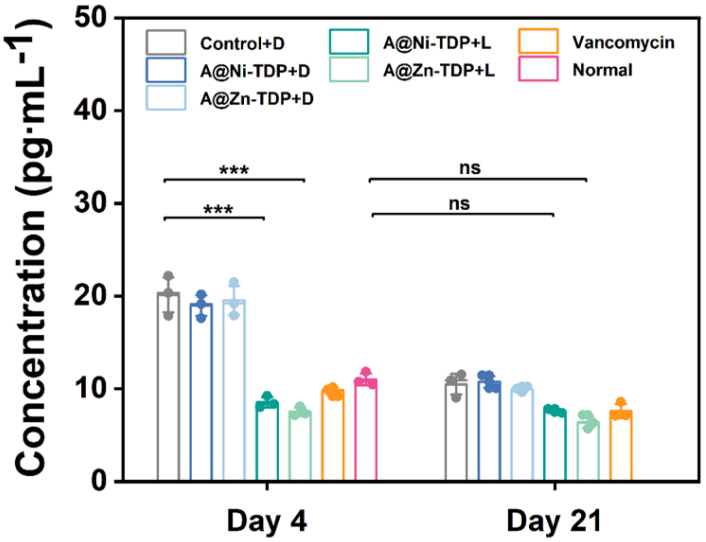

Figure S47. ELISA for the determination of MCP-1 in wound tissue of diabetic infected wounds on day 4 and 21 after different treatments.

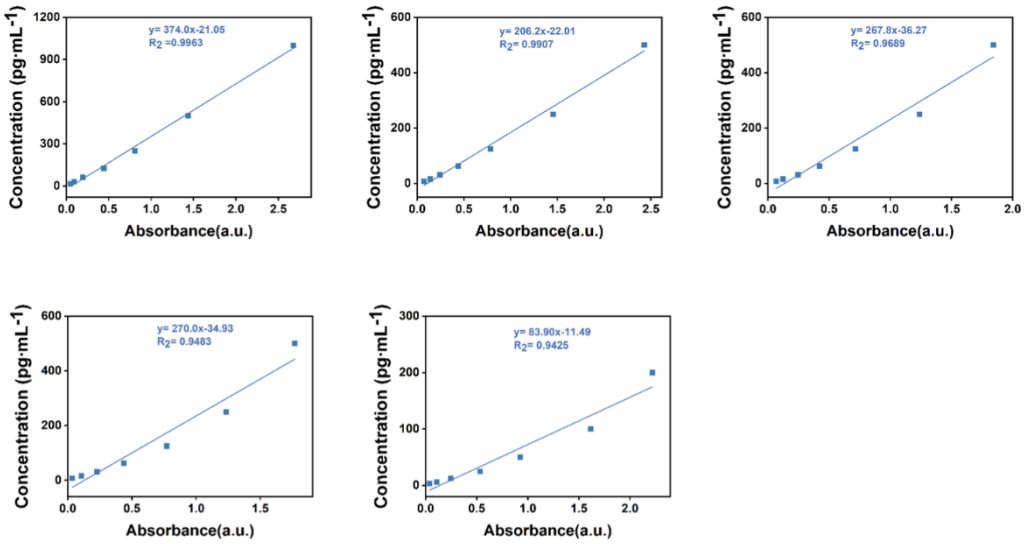

Figure S48. Standard curves for the determination of IL-6 (a), IL-10 (b), IL-1β (c), TNF-α (d), and MCP-1 (e) by ELISA.

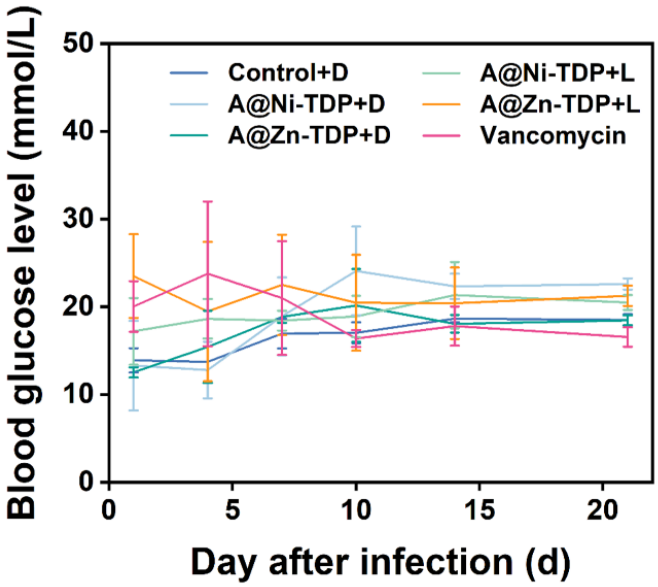

Figure S49. Changes in weight in diabetic infected wounds in 21 days after different treatments.

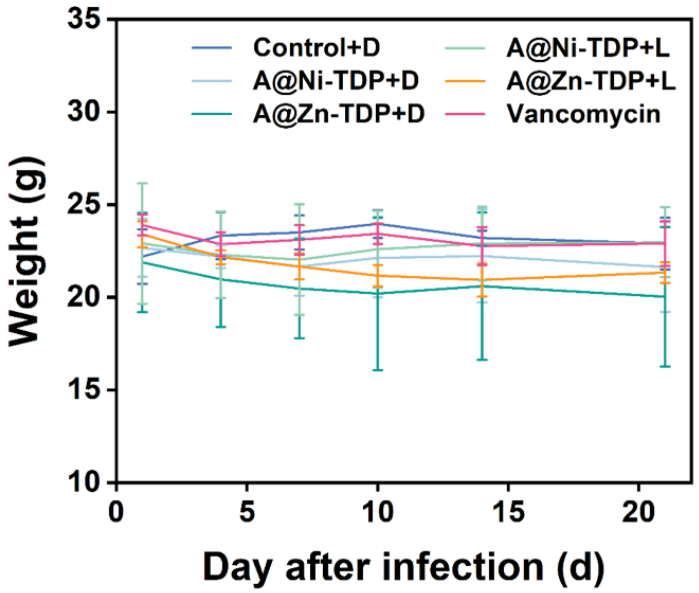

Figure S50. The levels of blood glucose changes (b) in diabetic infected wounds in 21 days after different treatments.

References

(1) Choi, S.-K.; Kim, J.; Kim, E. Overview of Syntheses and Molecular-Design Strategies for Tetrazine-Based Fluorogenic Probes. *Molecules* **2021**, *26* (7), 1868. https://doi.org/10.3390/molecules26071868.

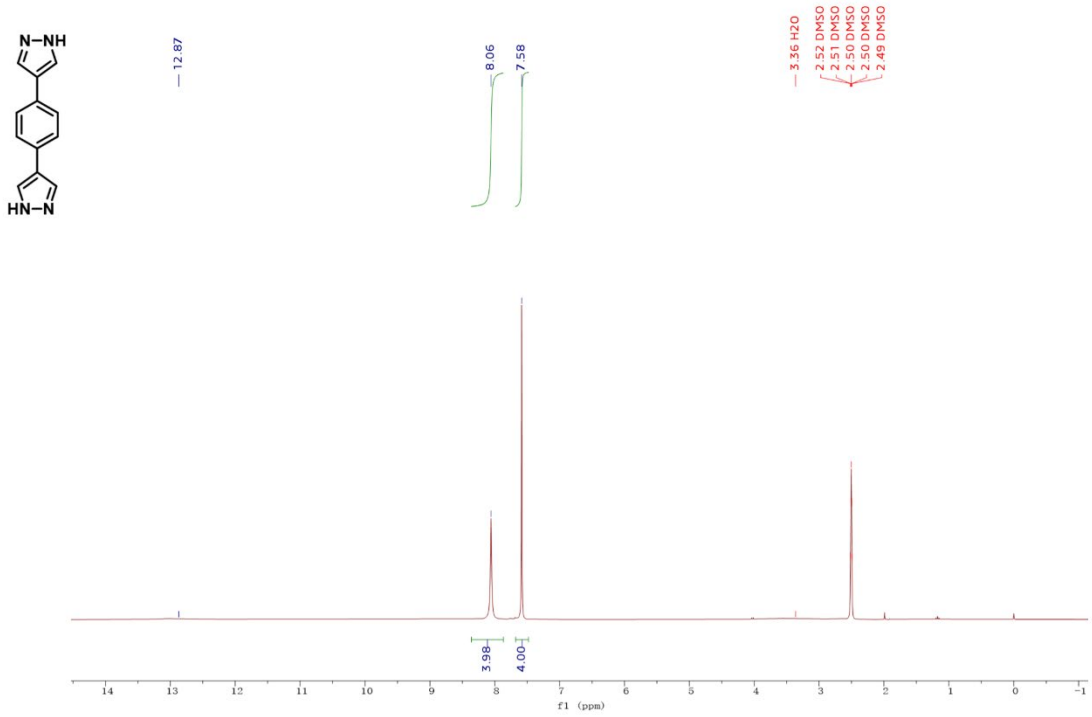
N–NH
HN–N
12.87
8.06
7.58
3.36 H2O
2.52 DMSO
2.51 DMSO
2.50 DMSO
2.50 DMSO
2.49 DMSO
3.98
4.00
14
13
12
11
10
9
8
7
6
5
4
3
2
1
0
−1
f1 (ppm)

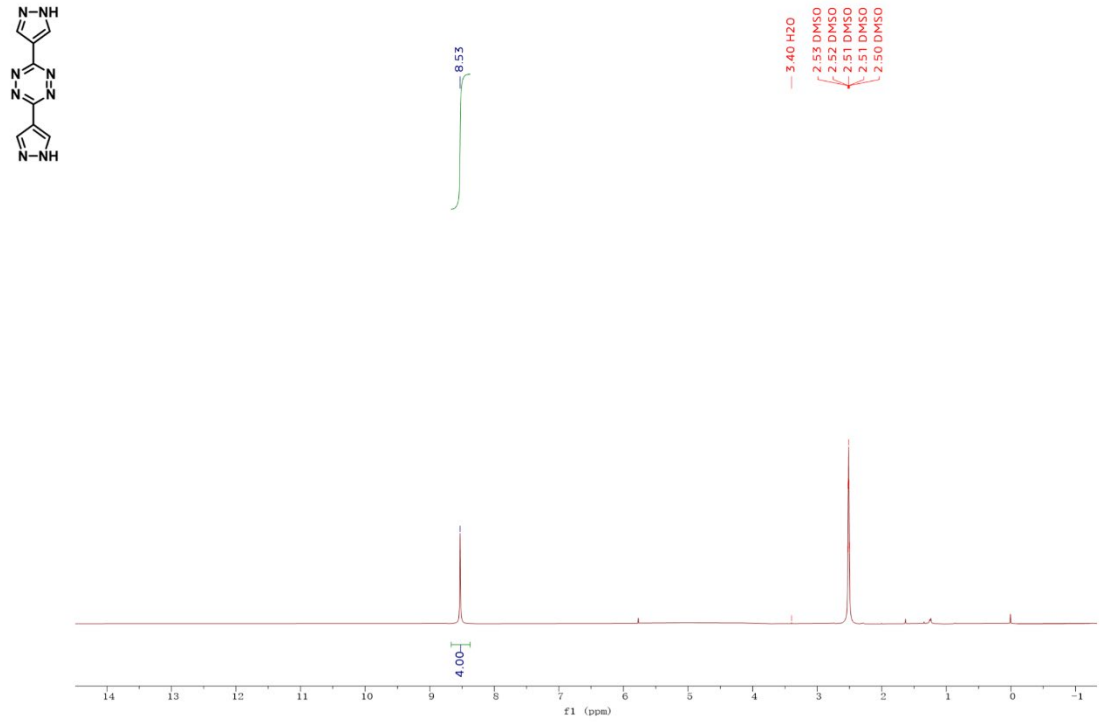

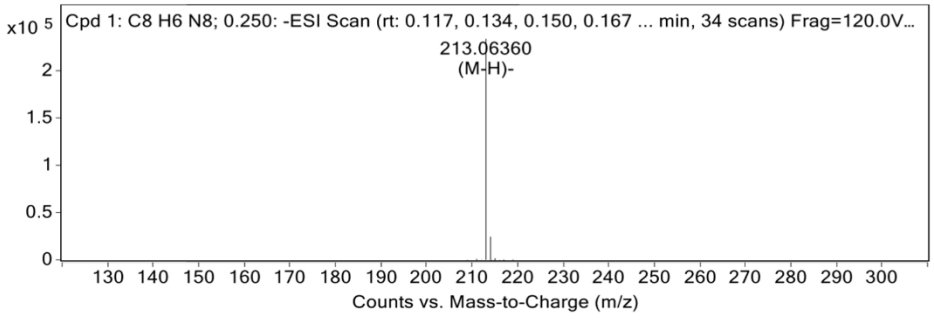

MS Spectrum Peak List

m/z	*Calc m/z*	Diff(ppm)	z	Abund	Ion
213.0636	213.06427	3.11	1	233554.61	(M-H)-
214.06545	214.06605	2.81	1	24454	(M-H)-
215.06714	215.06767	2.49	1	1392.26	(M-H)-